Molecular Cell

Article

FACT maintains chromatin architecture and thereby stimulates RNA polymerase II pausing during transcription *in vivo*

Graphical abstract

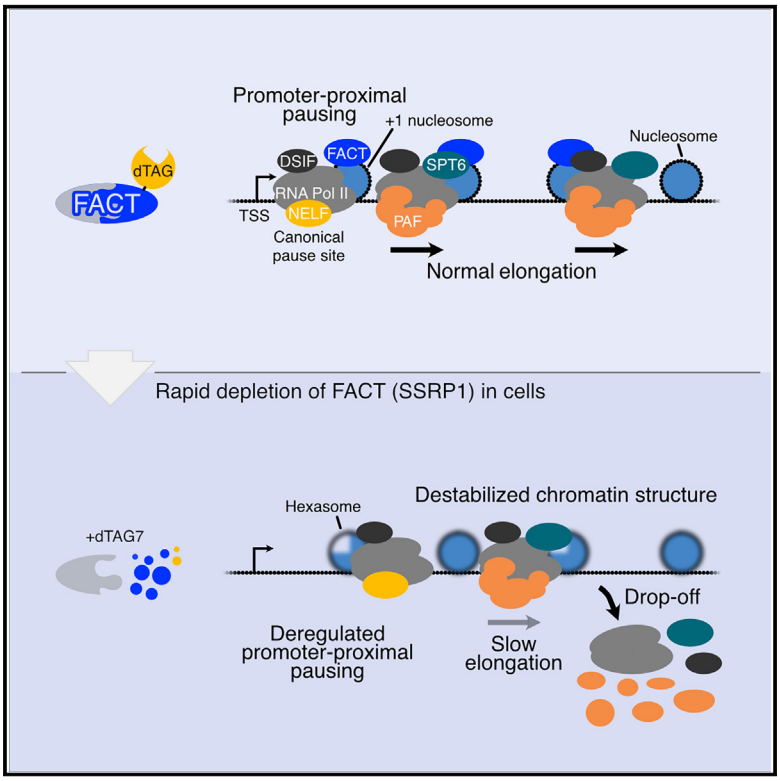

Highlights

- The histone chaperone FACT maintains chromatin structure in transcribed regions
- FACT has a positive role in transcription elongation *in vivo*
- Loss of FACT reduces RNA polymerase II elongation velocity and processivity
- FACT maintains +1 nucleosome integrity, which stabilizes promoter-proximal pausing

Authors

Kristina Žumer, Moritz Ochmann, Abrar Aljahani, ..., Ute Neef, A. Marieke Oudelaar, Patrick Cramer

Correspondence

kristina.zumer@mpinat.mpg.de (K.Ž.), marieke.oudelaar@mpinat.mpg.de (A.M.O.), patrick.cramer@mpinat.mpg.de (P.C.)

In brief

Žumer et al. investigate the mechanism by which the histone chaperone FACT regulates chromatin and transcription. They reveal multifaceted roles for FACT in maintaining chromatin architecture and controlling transcription at multiple stages of the transcription cycle. The authors also show that the +1 nucleosome, which depends on FACT, regulates transcription.

Žumer et al., 2024, Molecular Cell *84*, 1–17
June 6, 2024 © 2024 The Authors. Published by Elsevier Inc.
https://doi.org/10.1016/j.molcel.2024.05.003

CellPress

Please cite this article in press as: Žumer et al., FACT maintains chromatin architecture and thereby stimulates RNA polymerase II pausing during transcription *in vivo*, Molecular Cell (2024), https://doi.org/10.1016/j.molcel.2024.05.003

Molecular Cell

CellPress
OPEN ACCESS

Article

FACT maintains chromatin architecture and thereby stimulates RNA polymerase II pausing during transcription *in vivo*

Kristina Žumer,[1,4,*] Moritz Ochmann,[1,3] Abrar Aljahani,[2,3] Aiturgan Zheenbekova,[1,3] Arjun Devadas,[1] Kerstin Caroline Maier,[1] Petra Rus,[1] Ute Neef,[1] A. Marieke Oudelaar,[2,*] and Patrick Cramer[1,*]

[1]Max Planck Institute for Multidisciplinary Sciences, Department of Molecular Biology, Am Fassberg 11, 37077 Göttingen, Germany
[2]Max Planck Institute for Multidisciplinary Sciences, Genome Organization and Regulation, Am Fassberg 11, 37077 Göttingen, Germany
[3]These authors contributed equally
[4]Lead contact
*Correspondence: kristina.zumer@mpinat.mpg.de (K.Ž.), marieke.oudelaar@mpinat.mpg.de (A.M.O.), patrick.cramer@mpinat.mpg.de (P.C.)
https://doi.org/10.1016/j.molcel.2024.05.003

SUMMARY

Facilitates chromatin transcription (FACT) is a histone chaperone that supports transcription through chromatin *in vitro*, but its functional roles *in vivo* remain unclear. Here, we analyze the *in vivo* functions of FACT with the use of multi-omics analysis after rapid FACT depletion from human cells. We show that FACT depletion destabilizes chromatin and leads to transcriptional defects, including defective promoter-proximal pausing and elongation, and increased premature termination of RNA polymerase II. Unexpectedly, our analysis revealed that promoter-proximal pausing depends not only on the negative elongation factor (NELF) but also on the +1 nucleosome, which is maintained by FACT.

INTRODUCTION

Eukaryotic genomes are organized into nucleosomes, which consist of 147 base pairs (bp) of DNA that wrap 1.65 times around a histone octamer composed of one $(H3\text{-}H4)_2$ tetramer and two H2A-H2B dimers.[1] The packaging of eukaryotic DNA into chromatin poses a barrier for transcription since RNA polymerase II (RNA Pol II) needs to pass through many nucleosomes to transcribe a gene. Following transcription initiation, the elongating RNA Pol II often pauses in the promoter-proximal region of genes, just upstream of the +1 nucleosome. This is thought to function as an important checkpoint for the assembly of productive RNA Pol II elongation complexes (ECs).[2–5] The functional relationship between nucleosome architecture and promoter-proximal pausing, as well as the mechanisms that drive productive elongation through nucleosomes remain unclear. In addition, it remains incompletely understood how chromatin structure is maintained within actively transcribed regions.

RNA Pol II transcription is supported by chromatin remodelers and histone chaperones. The histone chaperone facilitates chromatin transcription (FACT) was identified and purified from nuclear extracts as a factor that stimulates transcription elongation on a chromatinized DNA template *in vitro*.[6] The human FACT complex is composed of two subunits: suppressor of Ty 16 (SPT16) and structure-specific recognition protein 1 (SSRP1),[7] whereas the yeast complex is composed of Spt16, polymerase one binding protein 3 (Pob3), and non-histone protein 6 (Nhp6).[8] These subunits form multiple interactions with all histone proteins and the DNA,[9] which require partial unwrapping of the nucleosomal DNA. This has been confirmed in a recent human FACT structure. This structure shows that FACT straddles the nucleosome and forms tight interactions with the histone core and DNA, which would clash with a complete nucleosome core particle.[10] It is therefore thought that FACT is recruited to actively transcribing genes by binding to nucleosomes that have been partially unwrapped by RNA Pol II. This is in line with *in vivo* mapping experiments in yeast[11,12] and with high-resolution structures of the yeast FACT complex bound to a nucleosome of which RNA Pol II has peeled off the first 40 bp of DNA. These structures show interactions between the FACT subunits and the partially unwrapped nucleosomes, but no direct interaction with RNA Pol II.[13,14]

Despite increasingly detailed structural insight, the precise function of FACT in regulating transcription and maintaining chromatin structure remains unclear. Biochemical and structural experiments have shown that FACT facilitates both nucleosome disassembly and reassembly and prevents loss of H2A-H2B dimers during RNA Pol II transcription *in vitro*.[14–20] To achieve this, it is thought that FACT binds to nucleosomes that have been partially unwrapped by RNA Pol II and facilitates the disassembly of these nucleosomes. It has been proposed that one H2A-H2B dimer is tethered to FACT and used for nucleosome reassembly after RNA Pol II has passed through. As FACT binds to the nucleosome, it competes with DNA and thus prevents re-binding of

This is an open access article under the CC BY license (http://creativecommons.org/licenses/by/4.0/).

Please cite this article in press as: Žumer et al., FACT maintains chromatin architecture and thereby stimulates RNA polymerase II pausing during transcription *in vivo*, Molecular Cell (2024), https://doi.org/10.1016/j.molcel.2024.05.003

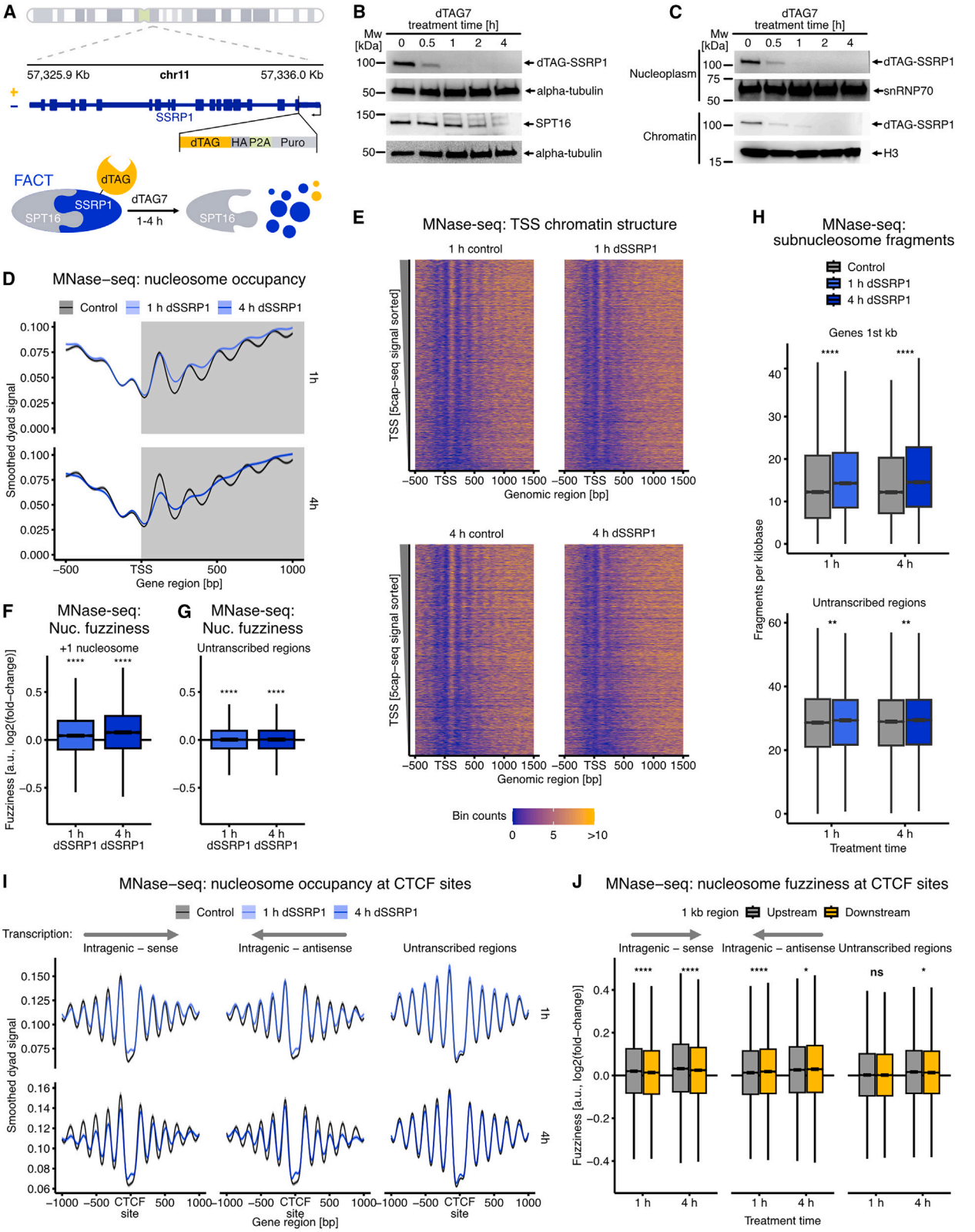

(legend on next page)

Please cite this article in press as: Žumer et al., FACT maintains chromatin architecture and thereby stimulates RNA polymerase II pausing during transcription *in vivo*, Molecular Cell (2024), https://doi.org/10.1016/j.molcel.2024.05.003

the unwrapped DNA to the nucleosome.[15–20] This model could therefore explain how FACT can promote the seemingly opposing processes of nucleosome disassembly during transcription and nucleosome reassembly without loss of H2A-H2B dimers following transcription (reviewed in Zhou et al.,[21] Formosa and Winston,[22] Jeronimo and Robert,[23] and Gurova et al.[24]).

This model fits well with the structural data described above and is consistent with enrichment of FACT at actively transcribed genes in both human cells and yeast.[11,25,26] However, it is not supported by functional *in vivo* studies. Several studies have shown that FACT perturbation does not lead to a significant reduction in transcription in eukaryotic cells.[26–32] It should be noted that a few studies have reported more substantive changes in gene expression following FACT inactivation. However, since the expression changes include both up- and down-regulation, do not correlate with changes in FACT occupancy, and are observed after long-term FACT perturbation, it is likely that they represent indirect effects.[25,33] Although evidence for a general reduction in transcription is lacking, several studies have identified more specific transcription defects after FACT perturbation, including cryptic transcription start site (TSS) selection in yeast[34–37] and reduced promoter-proximal pausing in flies.[38] By contrast, there is strong evidence for a central role for FACT in chromatin maintenance *in vivo* since several studies have shown that FACT inactivation leads to mislocalization and loss of nucleosomes in both yeast and human cells.[31,32,36–42] It has therefore been suggested that FACT primarily functions to preserve chromatin structure during transcription and does not have a prominent role in regulating transcription elongation (reviewed in Zhou et al.,[21] Formosa and Winston,[22] Jeronimo and Robert,[23] and Gurova et al.[24]).

A caveat of these studies addressing the role of FACT *in vivo* is that they are based on long-term ($\geq$24 h) perturbation of FACT. In addition, most studies use methods with relatively low sensitivity to detect transcription changes and without appropriate normalization strategies to identify potential global changes in transcription. To address these limitations, we have characterized the direct function of FACT *in vivo* and *in vitro* in detail by combining a multi-omics approach with biochemical experiments. To this end, we have monitored the effects of rapid FACT depletion on nucleosome structure, higher-order chromatin organization, RNA synthesis, and the occupancy of RNA Pol II and associated factors with a range of orthogonal high-resolution genomic techniques. Together, our data reconcile the currently conflicting roles for FACT that are observed in *in vitro* and *in vivo* experiments. In addition, our data show that RNA Pol II transcription is directly affected by changes in chromatin structure and vice versa, thus indicating a direct coupling of these processes.

RESULTS

Rapid FACT depletion destabilizes chromatin structure

To investigate the role of FACT *in vivo*, we generated a K562 cell line in which the SSRP1 subunit of FACT can be rapidly degraded with the use of the degradation tag (dTAG) system[43] (Figure 1A). We observed near-complete SSRP1 depletion following treatment with the dTAG7 ligand for 1 h and could no longer detect SSRP1 after 4 h of treatment (Figure 1B). SSRP1 is efficiently depleted from both nucleoplasm and chromatin (Figure 1C), and prolonged dTAG7 treatment also leads to decreased levels of the FACT subunit SPT16 (Figure 1B).

To examine the effects of rapid SSRP1 depletion on chromatin structure, we performed micrococcal nuclease digestion followed by deep sequencing (MNase-seq) after 1 and 4 h treatment with the dTAG7 ligand or corresponding control treatment with solvent only. To visualize nucleosome occupancy in genic

Figure 1. Rapid FACT depletion destabilizes chromatin structure

(A) Schematic representation of the edited endogenous *SSRP1* gene and dTAG rapid depletion system.

(B) Western blots of FACT subunits from lysates of cells treated with 500 nM dTAG7 for the indicated time. Alpha-tubulin is a loading control.

(C) Western blots of dTAGed SSRP1 from nucleoplasm and chromatin fraction of cells treated with 500 nM dTAG7 for the indicated time. snRNP70 and histone H3 are loading controls for nucleoplasmic and chromatin fraction, respectively.

(D) Metagene profiles showing mean smoothed dyad signal of MNase-seq upon SSRP1 depletion (dSSRP1, dTAG7 treatment) and control treatment, aligned at transcription start sites (TSSs) of genes (n = 4,681, see STAR Methods). The corresponding shaded area represents the 95% confidence interval of the mean. The gene region is shaded gray. The control samples are shown in black, and the dTAG7-treated samples are shown in the respective color. This color code is used throughout.

(E) Heatmap representations of nucleosome occupancy (MNase-seq) upon depletion of SSRP1 aligned at TSSs of genes (n = 4,681, see STAR Methods) and sorted by expression.

(F) Boxplots depicting changes in nucleosome fuzziness of +1 nucleosomes (n = 4,681). The thickened line represents the median fuzziness, the lower and upper hinges correspond to the first and third quartiles, respectively, and the notches extend to 1.58 times the interquartile range divided by the square root of n (~95% confidence interval). The whiskers represent the largest/smallest value within the 1.5 times interquartile range from the hinge, outliers are not shown. p values were determined with a one-sample two-sided Wilcoxon test (mu = 0) and are indicated for each treatment time. ns $p > 0.05$, * $p \leq 0.05$, ** $p \leq 0.01$, *** $p \leq 0.001$, **** $p \leq 0.0001$.

(G) Boxplots depicting changes in nucleosome fuzziness in untranscribed regions. Representations as in (F).

(H) Boxplots showing mean subnucleosomal fragment counts in genes (TSS to 1 kbp, n = 4,681) and untranscribed regions (n = 13,423) upon depletion of SSRP1. Counts were internally normalized for fragment content (see STAR Methods). Representations as in (F), except that p values were determined with two-sample Wilcoxon test.

(I) Metagene profiles showing mean smoothed dyad signal of MNase-seq upon SSRP1 depletion at intragenic and intergenic CTCF sites. Metagene profiles are aligned to the middle of CTCF sites according to the orientation of the CTCF motifs. Representations as in (D). Gray arrows indicate the direction of genic transcription.

(J) Boxplots depicting changes in nucleosome fuzziness upstream and downstream of CTCF sites. Representations as in (F). Gray arrows indicate the direction of genic transcription.

Please cite this article in press as: Žumer et al., FACT maintains chromatin architecture and thereby stimulates RNA polymerase II pausing during transcription *in vivo*, Molecular Cell (2024), https://doi.org/10.1016/j.molcel.2024.05.003

regions in these four conditions, we generated heatmaps and metaplots of the smoothed nucleosome dyad signal at constitutive TSSs (Figures 1D, 1E, and S1A), as well as at −1 nucleosome positions, pause sites, and +1 nucleosome positions (Figure S1B). In the control samples, we observed an expected nucleosome phasing pattern, characterized by a repetitive peak-valley signal in metagene profiles, which is typical for regions in which nucleosomes are regularly spaced and well-positioned. Upon SSRP1 depletion, this phasing pattern was less pronounced, with an initial increase of signal in the valleys after 1 h of depletion, which is combined with a decreased signal at the peaks after 4 h of depletion (Figures 1D and 1E).

Quantification of the changes in nucleosome position[44] shows that depletion of SSRP1 for 1 h leads to a small increase in the fuzziness of +1 nucleosomes and a further increase in fuzziness after 4 h of depletion (Figures 1F and S1C). By contrast, we observed minimal differences in nucleosome fuzziness in untranscribed regions (Figures 1G and S1D). Nucleosome phasing is stronger for highly expressed genes compared with lowly expressed genes (Figures 1E and S1E). In line with the observed increased fuzziness of the +1 nucleosome, FACT depletion also leads to a loss of phasing in the TSS region, which is more pronounced after a longer depletion time. To investigate whether the changes in chromatin structure in transcribed regions are associated with an enrichment of unwrapped nucleosomes, we quantified subnucleosomal fragments in the MNase-seq data. These fragments have been shown to correspond to unwrapped nucleosomal intermediates, including hexasomes.[45] In line with the changes in nucleosome fuzziness, this analysis shows that SSRP1 depletion leads to accumulation of unwrapped nucleosomes (which may correspond to hexasomes) in transcribed regions but only has a minimal effect on untranscribed regions (Figure 1H).

In line with previous findings,[46] we observed that binding sites of the zinc-finger protein CCCTC-binding factor (CTCF) are also associated with arrays of well-positioned nucleosomes (Figure S1F). This observation enabled us to further investigate the effect of FACT on chromatin structure within genes and untranscribed regions. We generated MNase-seq metaplots that are aligned with the orientations of the motifs contained within CTCF-binding sites and their orientations relative to RNA Pol II transcription. This results in an asymmetry in the MNase-seq pattern, with a more defined position for the nucleosome upstream of CTCF compared with the downstream nucleosome (Figure 1I). The metagene profiles show that depletion of SSRP1 causes a change in nucleosome positioning specifically in transcribed regions but has minimal impact on nucleosome architecture at CTCF-binding sites in untranscribed regions (Figure 1I). The effect of FACT depletion on nucleosome architecture at CTCF-binding sites is moderate compared with the observed changes at TSSs, which may reflect that these sites are less exposed to transcribing polymerases compared with the TSSs or that nucleosome positioning at CTCF-binding sites is also dependent on chromatin remodelers, such as imitation switch (ISWI) complexes.[47]

We observe that the effects of SSRP1 depletion are dependent on the direction of transcription. At CTCF-binding sites at which the orientation aligns with the direction of transcription, we observed a relatively strong reduction in the nucleosome phasing pattern upstream of CTCF and a weaker impact on the nucleosomes downstream; for CTCF-binding sites with an antisense orientation with respect to transcription, we observed the opposite effects. These observed asymmetric changes in metagene profiles are substantiated by asymmetric changes in nucleosome fuzziness (Figure 1J). This asymmetry could be explained by differential recruitment of chromatin remodelers to these upstream and downstream regions as RNA Pol II passes through. Together, our data confirm an important role for FACT in maintaining chromatin structure during transcription.[21–24]

A minor role for FACT in higher-order chromatin organization

Nucleosomes are further organized into higher-order chromatin structures, which include topologically associating domains (TADs) and compartments. TADs are formed by a loop extrusion process that is dependent on cohesin and CTCF, whereas compartments are thought to reflect the phase separation of euchromatin and heterochromatin.[48] To investigate how the observed changes in nucleosome positioning that result from SSRP1 depletion influence higher-order chromatin organization, we performed chromosome conformation capture (3C) experiments. To resolve patterns of genome folding at the level of individual nucleosomes, we utilized the Tiled-Micro-Capture-C technique (Tiled-MCC), which can generate local contact matrices of regions of interest at very high resolution.[49] We targeted several regions containing highly expressed genes in K562 cells (STAR Methods), including a subset of genes associated with previously characterized super-enhancers,[50] in cells treated with dTAG7 ligand or control for 4 h.

It has previously been shown that local chromatin folding patterns in gene bodies are characterized by fine-scale compartmentalization.[49] Depletion of SSRP1 leads to a general increase in interactions within gene bodies, which is indicative of a more compacted and less organized conformation in absence of FACT (Figures 2A and S2A). Regions surrounding CTCF-binding sites are characterized by a grid-like pattern of phased nucleosome arrays and strong insulation between the regions upstream and downstream.[49,51] SSRP1 depletion results in a less defined and fuzzier grid of nucleosomes at CTCF-binding sites contained within transcribed regions (Figures 2B and S2B). This is associated with a subtle decrease in local insulation, evident by the slight increase in interactions between the regions upstream and downstream of these CTCF-binding sites. Although we observed these effects at intragenic CTCF-binding sites throughout the targeted regions, we found that the local structures of intergenic CTCF-binding sites are not affected by SSRP1 depletion (Figure 2C).

We next investigated how the observed local changes in 3D chromatin architecture influence larger-scale features of genome organization by comparing contact matrices containing enhancer-dependent genes that are active in K562 cells in control- and dTAG7-treated cells. In contrast to previous observations,[52] we found that SSRP1 depletion does not lead to strong changes in the structure of TADs, subTADs, CTCF loops, and enhancer-promoter interactions (Figures 2D, S2C, and S2D). Together, this indicates that the role of FACT in maintaining

Please cite this article in press as: Žumer et al., FACT maintains chromatin architecture and thereby stimulates RNA polymerase II pausing during transcription *in vivo*, Molecular Cell (2024), https://doi.org/10.1016/j.molcel.2024.05.003

CellPress
OPEN ACCESS

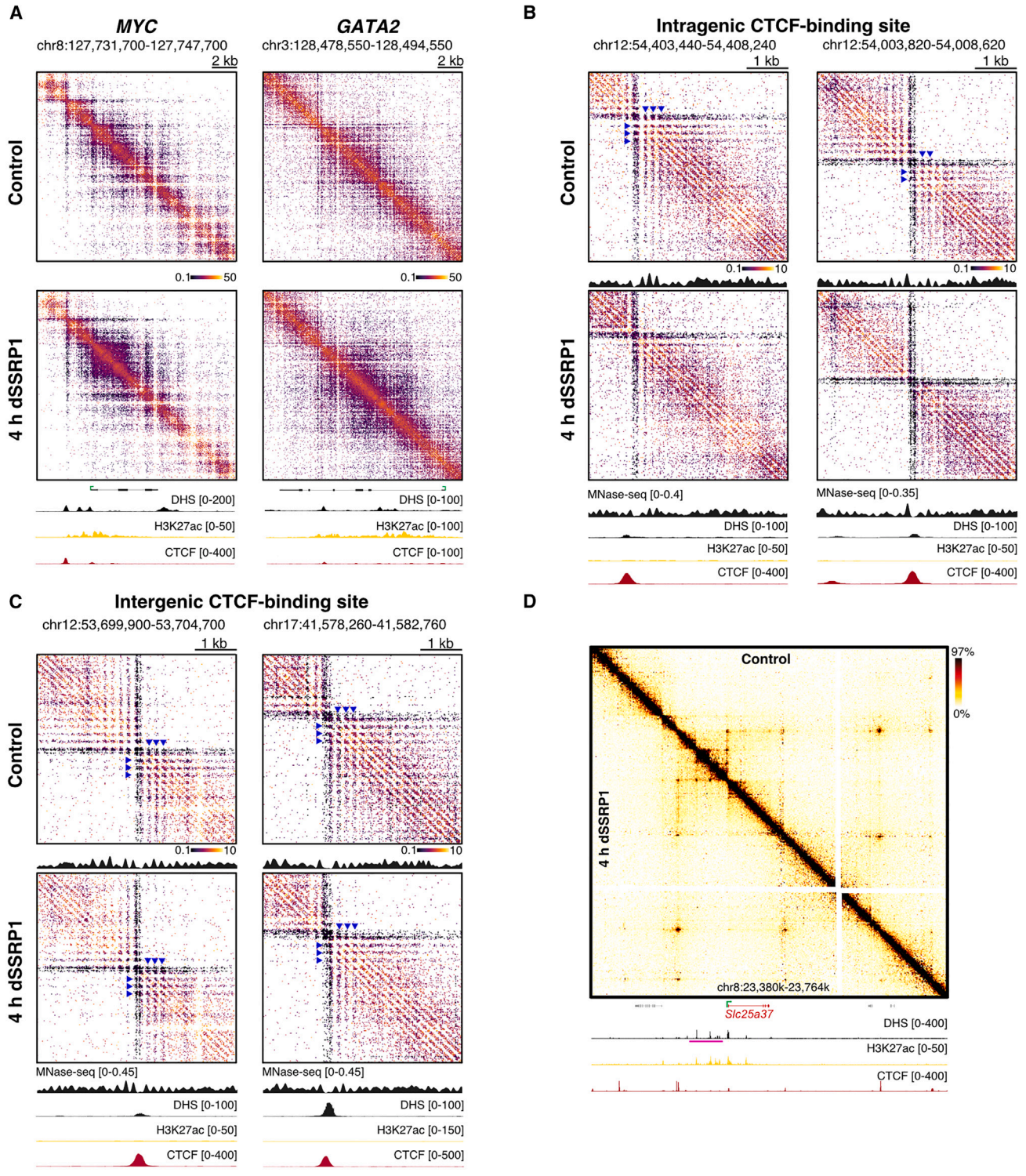

Figure 2. A minor role for FACT in higher-order chromatin organization

(A) Localized contact matrices (50 bp resolution) derived from Tiled-MCC ligation junctions of the *MYC* and *GATA2* loci in cells treated with solvent only (control, top) and dTAG7 ligand (dSSRP1, bottom). Gene annotation, DNase I hypersensitive sites (DHSs), and ChIP-seq tracks of H3K27ac and CTCF for wild-type K562 cells are shown at the bottom.

(legend continued on next page)

Please cite this article in press as: Žumer et al., FACT maintains chromatin architecture and thereby stimulates RNA polymerase II pausing during transcription *in vivo*, Molecular Cell (2024), https://doi.org/10.1016/j.molcel.2024.05.003

nucleosome architecture in transcribed regions contributes to the 3D organization of gene bodies and to local insulation at CTCF-binding sites but is not critical for the 3D organization of the genome at a larger scale.

FACT supports transcription elongation and processivity

To investigate the role of FACT in transcription, we performed transient transcriptome sequencing (TT-seq) after SSRP1 depletion. TT-seq combines metabolic RNA labeling with RNA fragmentation and isolation of labeled RNA for quantification of RNA synthesis.[53] To enable detection of global changes in RNA synthesis upon SSRP1 depletion, we used synthetic spike-ins for data normalization. In contrast to a recent study in mouse embryonic stem cells that suggests that FACT predominantly regulates tissue-specific genes,[54] we found that depletion of SSRP1 leads to a global reduction in RNA synthesis after 1 h of SSRP1 depletion and a further reduction after 4 h of depletion (Figures 3A and S3A). To further investigate the transcription defect and examine RNA synthesis within expressed genes, we generated metagene profiles of the TT-seq signal aligned at the TSSs and the transcript end sites (TESs) (Figure 3B). These analyses show that RNA synthesis is reduced throughout the gene body in the absence of FACT. Differential gene expression analysis identifies 657 downregulated genes and 54 upregulated genes after 1 h of SSRP1 depletion, and 3,703 downregulated genes and 157 upregulated genes after 4 h of SSRP1 depletion (Figure S3B). We found that depletion of SSRP1 leads to a decrease in transcription of all gene biotypes except for small nuclear RNAs (snRNAs) (Figure S3C). These results show that FACT has a predominantly stimulatory role on transcription in human cells.

To further investigate the transcription defect induced by SSRP1 depletion in human cells, we focused on RNA synthesis in the spatial context of expressed genes. In the TT-seq metagene profiles, we observed a small reduction in RNA synthesis at the 5′ ends of genes and a stronger decrease toward the 3′ ends upon 1 h of SSRP1 depletion (Figures 3B and S3D). After 4 h of depletion, RNA synthesis is strongly reduced at the 5′ ends of genes and even further decreased toward the 3′ ends. Notably, we observed an increase in the slope of the profile throughout the gene body for both depletion times. To further investigate this apparent elongation defect, we divided the expressed genes into four quantiles based on gene length (Q1–Q4; Figure 3C). Comparison of the TT-seq metagene profiles between these gene subsets uncovers interesting differences in the effects of SSRP1 depletion. After 1 h of depletion, the TT-seq signal for the shortest genes (Q1) is decreased, but there is no change in the shape of the profile. By contrast, we observe a clear increase in the slopes of the profiles for longer genes (Q2–Q4). After 4 h of SSRP1 depletion, the decrease in TT-seq signal across all gene subsets is stronger. In addition, we observed a stronger loss of signal toward the 3′ ends of long genes (Q4). To compare how different regions of genes are affected by FACT depletion, we determined the fold-change in RNA synthesis in 0.5 kb regions at the beginning (TSS), middle, and end of genes (Figure 3D). This analysis recapitulated the changes observed in metagene profiles upon FACT depletion (Figure 3B), in which the effect of FACT depletion progressively increases from the 5′ end to the 3′ end of the metagene profiles. The same pattern is visible when we separate genes into gene length subsets, although it is more pronounced in the longer gene subsets (Figure 3E). RNA synthesis in TSS-proximal regions is least affected by FACT depletion and does not pass the significance cutoff ($p \geq 0.05$). In line with this, we observe a stronger reduction in RNA synthesis for long genes (Figure S3E) but also for highly expressed genes (Figure S3F). Taken together, these effects are similar to the transcription defect that has previously been described in the context of depletion of the elongation factor SPT6[55] and indicate that FACT acts as a positive regulator of transcription elongation.

To investigate whether the effects of SSRP1 depletion on transcription elongation are accompanied by changes in RNA Pol II processivity, we examined changes in occupancy of transcriptionally engaged RNA Pol II using mammalian nascent elongating transcript sequencing (mNET-seq) after SSRP1 depletion.[56] mNET-seq maps the last nucleotide incorporated into RNA molecules that are associated with transcribing RNA Pol II and therefore provides strand-specific information about RNA Pol II occupancy with single nucleotide resolution. The mNET-seq data show that depletion of SSRP1 for 1 h leads to a major redistribution of transcriptionally engaged RNA Pol II in gene bodies (Figures 3F, S3G, and S3H). In the SSRP1-depleted cells, the mNET-seq signal is increased in the beginning of genes (~1–3 kbp) and decreased further in the gene bodies. This pattern is amplified after 4 h of SSRP1 depletion.

The observed accumulation of engaged RNA Pol II in the 5′ regions of genes following SSRP1 depletion could be explained by an increase in transcription in these regions or by a defect in RNA Pol II progression into gene bodies. These two possibilities can be distinguished by calculating the elongation velocity of RNA Pol II. We have previously shown that RNA synthesis per transcribing RNA Pol II, calculated as the ratio of RNA synthesis (TT-seq) and RNA Pol II occupancy (mNET-seq), can be used as a proxy for RNA Pol II elongation velocity.[55,57] To estimate changes in elongation velocity after depletion of SSRP1, we tiled the human genome into 50 bp bins, calculated the TT-seq/mNET-seq ratio per bin, and generated a heatmap that shows the changes in this ratio for all expressed genes upon SSRP1 depletion (Figure 3G). This analysis shows that RNA Pol II accumulation in the 5′ regions of genes is associated with a reduction in elongation velocity, indicating a defect in RNA Pol II progression into gene bodies. Of note, 4 h depletion of SSRP1 leads to very low mNET-seq signals toward the 3′ region of genes

(B) Localized contact matrices (20 bp resolution) derived from Tiled-MCC ligation junctions of intragenic CTCF-binding sites in cells treated with solvent only (control, top) and dTAG7 ligand (dSSRP1, bottom). Annotation as in (A), including MNase-seq data of the control-treated sample.
(C) Localized contact matrices (20 bp resolution) derived from Tiled-MCC ligation junctions of intergenic CTCF-binding sites. Representations as in (B).
(D) Tiled-MCC contact matrices (2 kb resolution) of the *Slc25a37* locus in cells treated with solvent only (control, top right) and dTAG7 ligand (dSSRP1, bottom left). The region highlighted in magenta indicates *Slc25a37* enhancers. Annotation as in (A).

Please cite this article in press as: Žumer et al., FACT maintains chromatin architecture and thereby stimulates RNA polymerase II pausing during transcription *in vivo*, Molecular Cell (2024), https://doi.org/10.1016/j.molcel.2024.05.003

CellPress
OPEN ACCESS

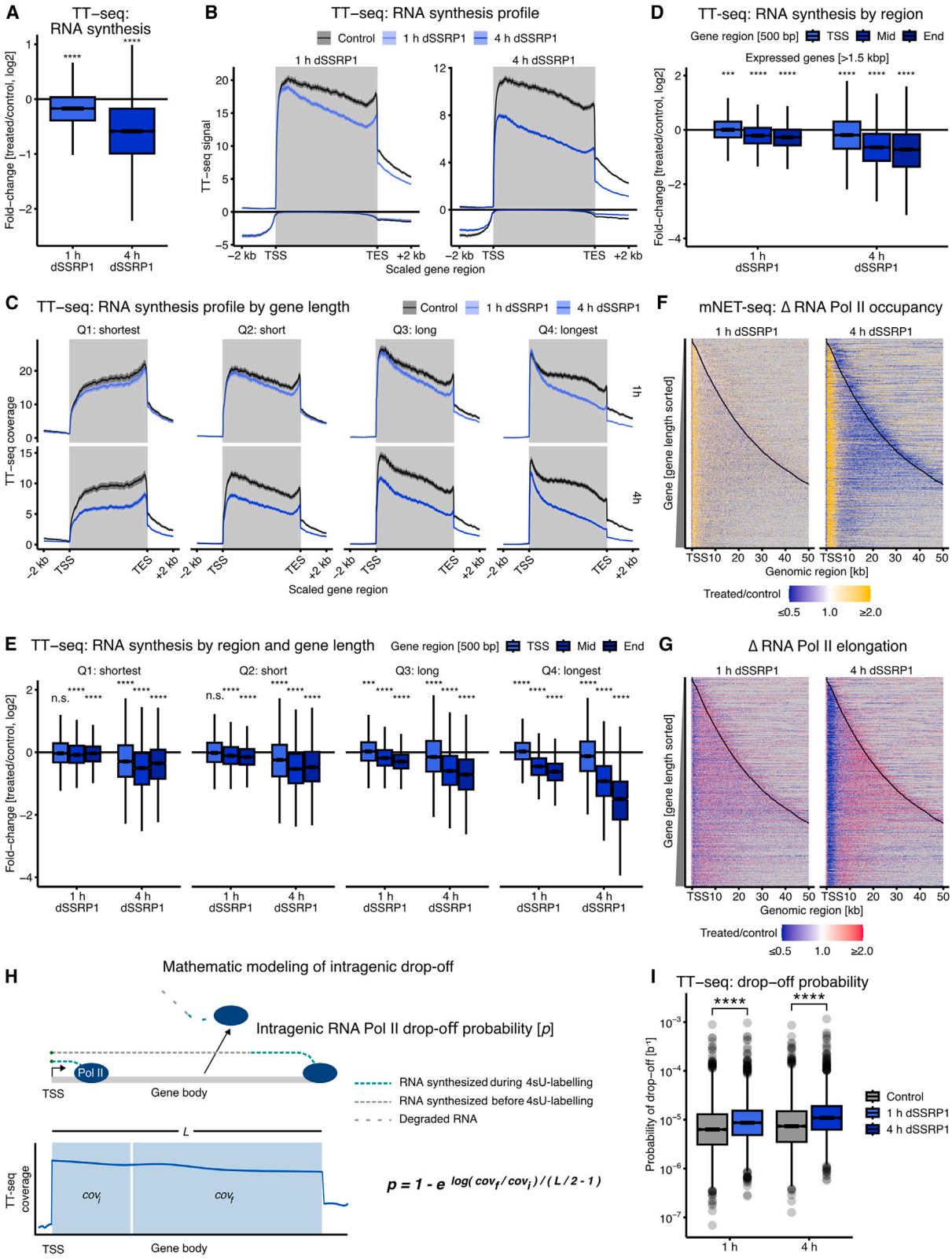

(legend on next page)

Please cite this article in press as: Žumer et al., FACT maintains chromatin architecture and thereby stimulates RNA polymerase II pausing during transcription *in vivo*, Molecular Cell (2024), https://doi.org/10.1016/j.molcel.2024.05.003

(Figure S3H), which limits analysis of velocity in promoter-distant regions (beyond 10 kb from the TSS) of genes.

The loss of engaged RNA Pol II in the 3′ regions of genes following SSRP1 depletion could be explained by increased drop-off of RNA Pol II in absence of FACT. To investigate this, we devised a mathematical model to quantify the drop-off probability per gene based on the TT-seq signal (Figure 3H; STAR Methods). We postulate a random negative binomial drop-off likelihood throughout the gene, based on the assumption that RNA Pol II can drop off at any position in the gene, and the resulting decrease in the TT-seq signal can be expressed in terms of the length of the gene and the per-base drop-off probability. We found that the mean drop-off probability per base within a gene is significantly increased after 1 h of SSRP1 depletion and further increased after 4 h of depletion (Figure 3I), which is in line with the observed loss of RNA Pol II occupancy in gene bodies (Figure 3F). In agreement with the metagene profiles for different length classes, the depletion of FACT has less effect on drop-off probability for short genes (bottom 25% of genes by length) than long genes (top 25% of genes by length), but the difference is significant for both length classes (Figure S3I). Taken together, FACT is not only required for RNA Pol II elongation but also for processivity, preventing RNA Pol II drop-off by premature termination.

FACT depletion perturbs promoter-proximal transcription

To explore the molecular mechanism underlying defective RNA Pol II progression in the 5′ regions of genes in the absence of FACT, we investigated the effects of SSRP1 depletion on transcription in the promoter-proximal region in more detail. To this end, we first determined the positions of promoter-proximal RNA Pol II pausing and the +1 nucleosome dyads in control-treated cells. We find the pause site position distribution peaks at ∼45 bp and the +1 nucleosome dyad position distribution peaks at ∼120 bp relative to the TSS (Figure 4A). We next generated heatmaps showing the change in RNA Pol II occupancy near the TSSs of all paused genes, sorted by the distance between the pause sites and the TSSs (Figure 4B). Interestingly, this shows that there is a strong loss of RNA Pol II occupancy near the TSS, which precedes the notable accumulation of RNA Pol II downstream of the promoter-proximal pause site (compare Figure 4B to Figure 3F). In contrast to observations in yeast,[34–37] we did not observe a notable appearance of cryptic TSSs with 5′ cap-seq in the absence of FACT (Figures S4A–S4C). This finding indicates that the loss of promoter-proximal RNA Pol II occupancy is not due to defective TSS selection.

To investigate the redistribution of RNA Pol II in the absence of FACT in detail, we used the determined TSSs, pause sites, and +1 nucleosome dyad positions within each gene to generate metagene profiles of RNA Pol II occupancy anchored at the TSSs, pause sites, and +1 nucleosomes (Figure 4C). These profiles show that the occupancy of RNA Pol II as detected by mNET-seq is highest at the pause sites, which are ∼45 bp downstream of the TSSs. Following both 1 and 4 h SSRP1 depletion, we observed a strong loss of RNA Pol II at the pause sites (Figures 4C and 4D). The mNET-seq profiles anchored at the TSSs and +1 nucleosome positions show that the reduction in RNA Pol II at the pause sites after SSRP1 depletion is followed by an increase in signal above control further downstream of the TSS (∼120 bp) in a region within the +1 nucleosome that is in close proximity to the annotated dyad. This pattern of RNA Pol II redistribution is the same for 1 and 4 h depletion of SSRP1, although the changes are more pronounced after 4 h treatment.

To confirm that the changes in mNET-seq signal reflect a redistribution of paused RNA Pol II complexes, we examined the distribution of the negative elongation factor (NELF), which stabilizes promoter-proximal pausing, and RNA Pol II. We performed chromatin immunoprecipitation sequencing (ChIP-seq) with antibodies against NELF subunits NELF-C/D and the N terminus of the largest subunit of RNA Pol II (Figures 4E–4G and S4D–S4I). This shows that loss of SSRP1 leads to a decrease in ChIP-seq signal for RNA Pol II and NELF at the pause sites and an increased signal downstream of the pause sites that extends into the gene bodies. In line with the observed reduction of transcriptionally engaged RNA Pol II as measured by mNET-seq, these data show that loss of FACT leads to a reduction of promoter-proximal RNA Pol II pausing in the canonical pausing window (Figure 4), which is followed by an increase in NELF-associated RNA Pol II downstream of the pause sites as a result of defective progression of RNA Pol II into gene bodies (Figure 3).

Figure 3. FACT supports transcription elongation and processivity

(A) Boxplots showing RNA synthesis fold change (TT-seq) of all expressed genes (n = 8,965) upon SSRP1 depletion. Representations as in Figure 1F.

(B) Scaled metagene profiles of TT-seq signal showing mean signal of expressed genes (n = 8,965) after depletion of SSRP1. Representations as in Figure 1D, except that the metagene profile is scaled between the TSS and TES and includes unscaled regions upstream and downstream of the gene. The sense and antisense profiles are shown as positive and negative values, respectively.

(C) Scaled metagene profiles of TT-seq signal showing mean signal of expressed genes (n = 8,965) separated into gene length quartiles after depletion of SSRP1 (Q1: 50 bp–11 kbp; Q2: 11–27 kbp; Q3: 27–62 kbp; and Q4: 62–1,113 kbp). Representations as in (B), except that only sense profiles are shown.

(D) Boxplots showing RNA synthesis fold change (TT-seq) of 0.5 kb gene regions (TSS, mid, and end) of expressed genes longer than 1.5 kb upon SSRP1 depletion. Representations as in Figure 1F.

(E) Boxplots showing RNA synthesis fold change (TT-seq) of TSS, mid, and end regions of genes in gene length subsets from (C). Representations as in (D).

(F) Heatmap representations of changes in RNA Pol II occupancy upon depletion of SSRP1. Expressed gene (n = 8,965) regions are aligned at the TSS and sorted by gene length. The black line represents the gene end, and bins without signal are shown in light gray.

(G) Heatmap representations of changes in elongation velocity upon depletion of SSRP1. Representations as in (F).

(H) Schematic of mathematical modeling of RNA Pol II drop-off probability (p) based on TT-seq signal in the 5′ regions (cov_i) and the signal in the gene body (cov_f) for a gene of length L.

(I) Boxplots showing mean per base probability of RNA Pol II drop-off of expressed genes (L > 3.5 kbp and $cov_i > cov_f$; n = 3,190, see STAR Methods). Representations as in Figure 1H.

Please cite this article in press as: Žumer et al., FACT maintains chromatin architecture and thereby stimulates RNA polymerase II pausing during transcription *in vivo*, Molecular Cell (2024), https://doi.org/10.1016/j.molcel.2024.05.003

CellPress
OPEN ACCESS

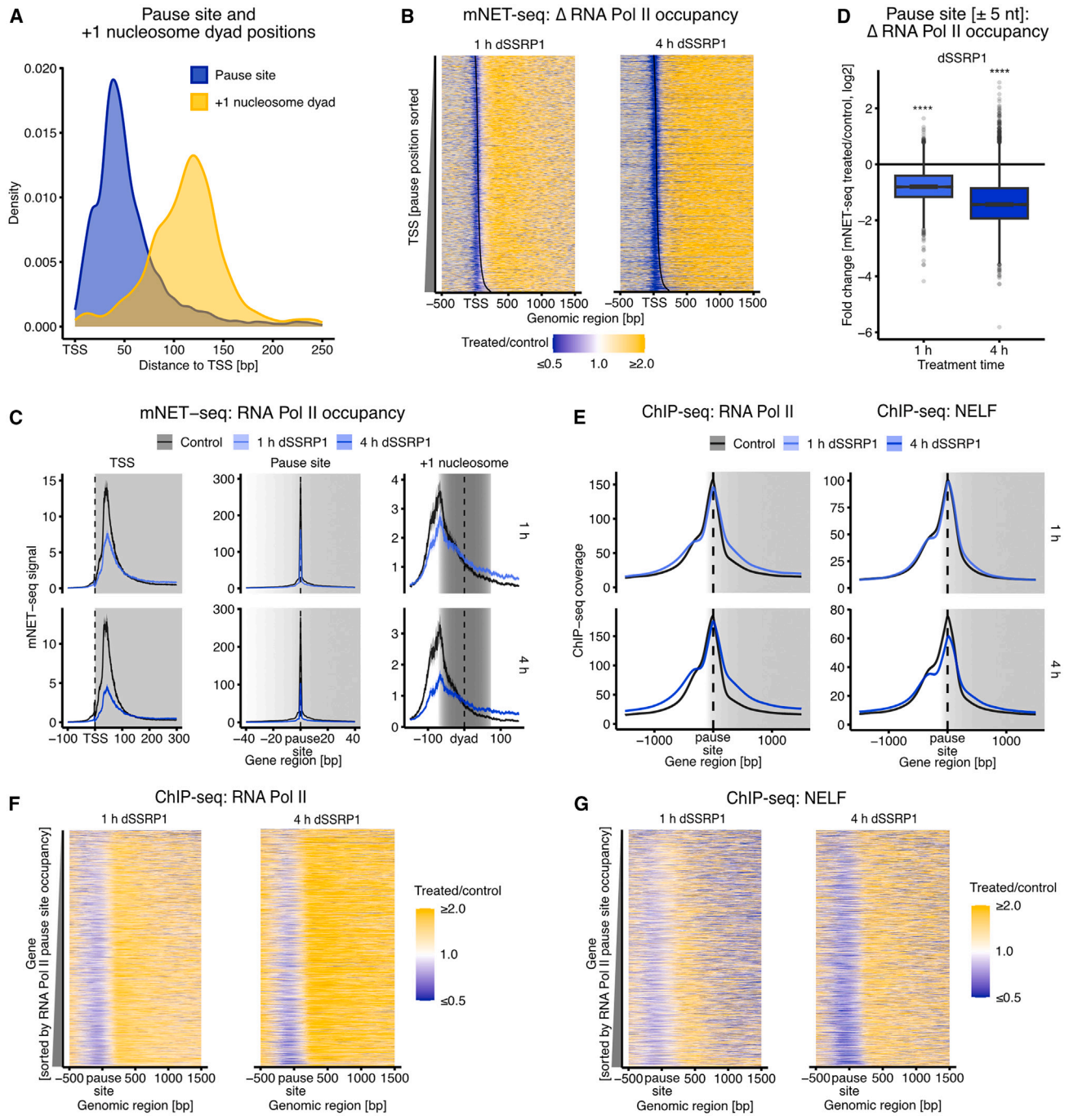

Figure 4. FACT depletion perturbs promoter-proximal transcription

(A) Density plot showing the distribution of the pause positions and +1 nucleosome dyad distances to TSS (see STAR Methods). Values above 250 bp are not shown.

(B) Heatmap representations of changes in RNA Pol II occupancy of expressed genes with a pause site (n = 4,681). Gene regions are anchored at the TSS and sorted by the pause position. The black line represents the pause site, and bins lacking signal are shown in light gray.

(C) Metagene profiles aligned at the TSS (left), promoter-proximal pause site (middle), and +1 nucleosome dyad (right) showing mean occupancy of RNA Pol II (mNET-seq) upon SSRP1 depletion. Representations as in Figure 1D and only sense profiles are shown (n = 4,681). Nucleosome region is shaded dark gray.

(D) Boxplots showing change in RNA Pol II occupancy (fold-change of mNET-seq signal) at the pause site (n = 4,681) upon depletion of SSRP1. Representations as in Figure 1F.

(legend continued on next page)

Please cite this article in press as: Žumer et al., FACT maintains chromatin architecture and thereby stimulates RNA polymerase II pausing during transcription *in vivo*, Molecular Cell (2024), https://doi.org/10.1016/j.molcel.2024.05.003

Taken together with the observed reduction in RNA Pol II velocity in the beginning of genes (Figure 3G), these results indicate that the observed RNA Pol II accumulation downstream of the pause site does not represent pause-released, actively elongating RNA Pol II but represents NELF-bound RNA Pol II corresponding to a paused EC, which is not accurately paused at the canonical pause site.

FACT reduces the nucleosome barrier to RNA Pol II

To further investigate how loss of FACT leads to an apparent loss in promoter-proximal RNA Pol II pausing, we devised a biochemical system composed of purified proteins and a DNA template to analyze promoter-proximal RNA Pol II pausing *in vitro*. To this end, we performed RNA elongation assays with the early EC (composed of RNA Pol II and DRB sensitivity-inducing factor (DSIF)) and transcription factor IIS (TFIIS) using either a linear DNA template or a DNA template wrapped around a single nucleosome (Figures 5A and S5A–S5C). In this setup, we first tested how the inclusion of NELF in the reaction affects transcription. We observed that the presence of NELF leads to a decrease in the full-length product transcribed from a linear DNA template (Figures 5B, 5C, and S5A–S5D), which is in agreement with previous observations.[58] The inclusion of a nucleosome on the DNA template leads to the appearance of two distinct intermediate products (°, °°) and a reduction in the production of full-length product. The shorter intermediate (°) is 60 nt in length and corresponds to positioning of the RNA Pol II active site at the edge of the downstream nucleosome. The longer intermediate (°°) corresponds to an RNA Pol II position at which it has transcribed ~6 turns of nucleosomal DNA and elongated the RNA to 127 nt. This intermediate appears equivalent to the intermediate at the nucleosome dyad generated by the activated EC.[59]

Increasing the NELF concentration leads to less formation of the full-length and the longer intermediate (°°) product and a concomitant increase of the shorter intermediate (°) product (Figures S5A and S5B). This indicates that there is an increased nucleosome entry barrier when NELF is included in the reaction (Figures 5D, S5E, and S5F). The distance of the RNA Pol II active site for the shorter intermediate (°) relative to the nucleosome dyad is 75 bp. This closely matches the observed distance between the RNA Pol II promoter-proximal pause site and the +1 nucleosome dyad in human cells (Figure 4A). These data suggest that the shorter intermediate (°) product corresponds to the *in vivo* RNA Pol II pause site position, at which NELF stabilizes promoter-proximal pausing in the region upstream of the +1 nucleosome.[60] We therefore conclude that RNA Pol II pausing *in vitro* is stabilized by both NELF and the +1 nucleosome.

We next used this experimental setup to measure the effect of FACT on promoter-proximal pausing of RNA Pol II *in vitro*. We find that the addition of FACT to the *in vitro* transcription experiments does not affect RNA production from the linear DNA template (Figures 5E and S5D). By contrast, inclusion of FACT in an *in vitro* transcription reaction in which the DNA is wrapped around a histone octamer leads to an increase in the full-length product due to a decrease of the dyad barrier (Figures 5E, 5F, S5D, and S5G). Interestingly, we observe that the addition of FACT to reactions with a nucleosome template does not affect RNA Pol II accumulation at the pause site (°) and the nucleosome entry barrier (Figures 5E and 5G). Taken together, these observations suggest that FACT stimulates transcription of the early EC by lowering the barrier at the dyad of the nucleosome but does not release paused RNA Pol II.

To test how the NELF-containing paused EC transcribes a hexasome-containing template, we performed *in vitro* transcription reactions in the presence and absence of both NELF and FACT with a DNA template wrapped around a histone hexamer (Figures 5B, 5E, and S5C–S5G). Notably, we observed less production of the pausing intermediate (°) at the edge of the hexasome compared with the edge of the complete nucleosome, which indicates that the presence of a complete histone octamer leads to more RNA Pol II pausing compared with a hexamer (Figures 5D and S5F). As for the complete histone octamer, the entry barrier is further stabilized by NELF. In line with the experiments with the nucleosome-containing template, the addition of FACT to the hexasome-containing template increases the yield of full-length product and decreases the production of the longer intermediate (°°), which suggests that FACT also stimulates the progression of Pol II through hexasomes. This indicates that FACT does not only stimulate transcription by destabilization of H2A/H2B dimers, as has been suggested,[21] but also by other mechanisms. In summary, the differences between transcription through a hexasome or a nucleosome *in vitro* indicate that the observed enrichment of subnucleosomal fragments (which may correspond to hexasomes) in expressed genes near the TSSs upon SSRP1 depletion (Figure 1H) could explain the observed pausing defect and leakage of paused ECs into the genes (Figure 4) in cells in the absence of FACT.

DISCUSSION

In this study, we have generated a human cell line that allows for rapid depletion of FACT. We have used a combination of high-resolution genomic approaches in these cells, together with biochemical *in vitro* experiments, to provide detailed insight into the role of FACT in regulating chromatin structure and transcription (Figures 6A and 6B).

Our analyses of chromatin architecture following FACT depletion show that FACT regulates nucleosome integrity in transcribed regions, thus confirming an important role for FACT in maintaining chromatin structure during transcription.[21–24] In contrast to a recent report showing a function for FACT in the regulation of interactions between gene promoters and

(E) Metagene profiles aligned at the pause site showing ChIP-seq signal of RNA Pol II and NELF-C/D upon SSRP1 depletion (n = 4,681). Representations as in Figure 1D.

(F) Heatmap representations of changes in RNA Pol II ChIP-seq signal of expressed genes with a pause site (n = 4,681). Gene regions are anchored at the pause site and sorted by RNA Pol II signal at the pause site. Bins lacking signal are shown in light gray.

(G) Heatmap representations of changes in NELF-C/D ChIP-seq. Representations as in (F).

Please cite this article in press as: Žumer et al., FACT maintains chromatin architecture and thereby stimulates RNA polymerase II pausing during transcription *in vivo*, Molecular Cell (2024), https://doi.org/10.1016/j.molcel.2024.05.003

CellPress
OPEN ACCESS

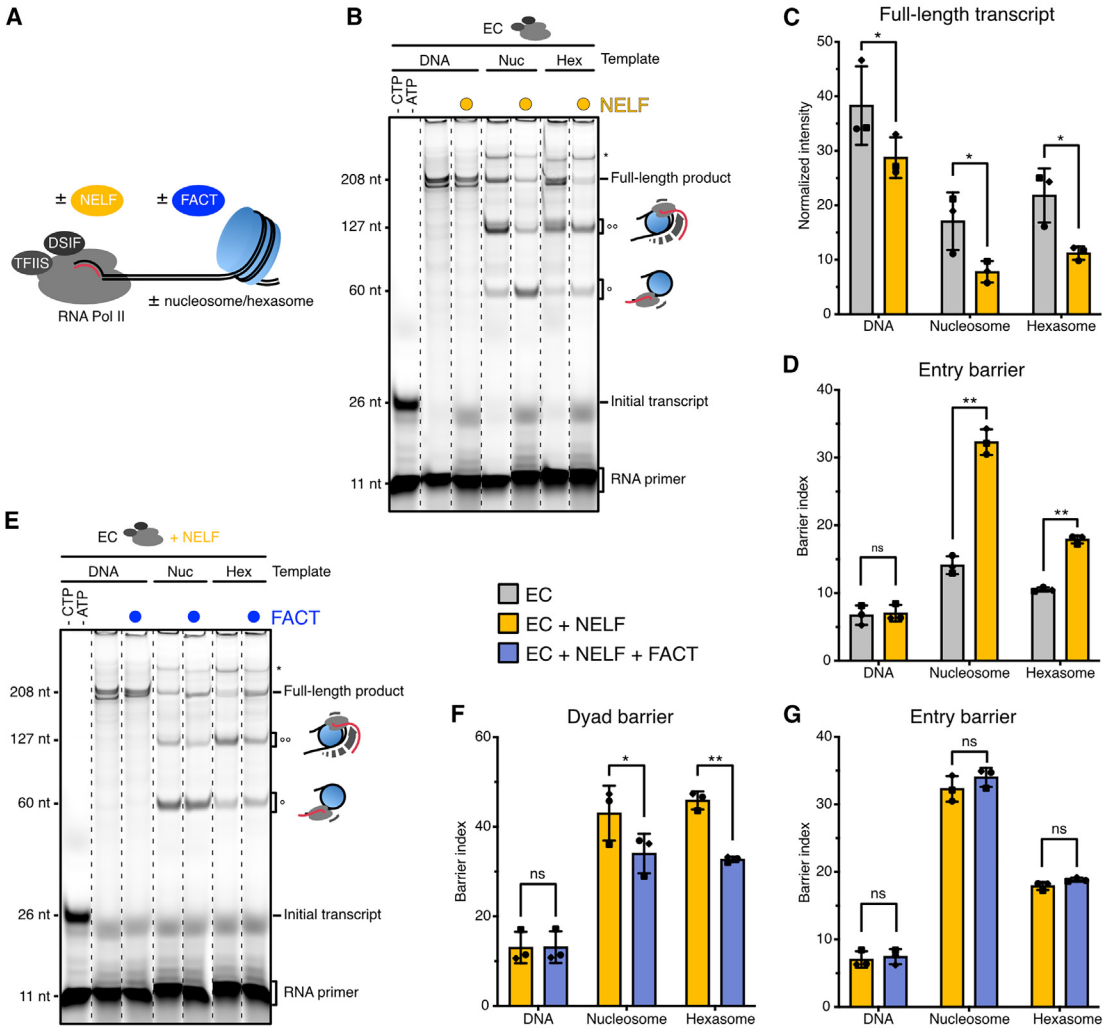

Figure 5. FACT reduces the nucleosome barrier to RNA Pol II

(A) Schematic of the *in vitro* RNA elongation assay with an early elongation complex (EC) and additional factors. The assay was performed with three DNA templates and a fluorescently labeled RNA primer (red).

(B) Denaturing polyacrylamide gel electrophoresis (PAGE) separation of RNA elongation assay products showing the effect of NELF on *in vitro* transcription of three templates. Templates are linear DNA (DNA), DNA wrapped around a complete histone octamer (Nuc), or histone hexamer (Hex). First lane shows product without addition of CTP and ATP. The schematics of RNA Pol II and the nucleosome depict the corresponding states. Results are representative of 3 independent experiments. Non-specific product is marked (*). Selected lanes from Figures S5A–S5C are shown, and dashed lines mark cropped lanes.

(C) Bar chart showing quantification of the full-length product of RNA elongation assays shown in (B). The mean normalized intensities per condition are shown with error bars (±SD) and points for each measured value. Point shapes represent the independent experiments. The effect of NELF addition was tested with paired t test ($n = 3$; ns $p > 0.05$, * $p \leq 0.05$, ** $p \leq 0.01$, *** $p \leq 0.001$, **** $p \leq 0.0001$).

(D) Bar chart showing quantification of the entry barrier of RNA elongation assays shown in (B) (see Figure S5D and STAR Methods). Representations as in (C).

(E) Denaturing PAGE of RNA elongation assay products showing the effect of FACT on transcription by EC in the presence of NELF. Representations as in (B).

(F) Bar chart showing quantification of the dyad barrier of RNA elongation assays shown in (E). Representations as in (C).

(G) Bar chart showing quantification of the entry barrier of RNA elongation assays shown in (E). Representations as in (C).

enhancers,[52] we did not observe clear changes in enhancer-promoter interactions. This discrepancy may be explained by differences in depletion times, namely, 24 h compared with 4 h in our study.

By investigating the effects of rapid FACT depletion on transcription, we demonstrate that FACT plays a critical role in promoting transcription through chromatin *in vivo*. These observations are in contrast with previous reports (reviewed in Zhou et al.,[21] Formosa and Winston,[22] Jeronimo and Robert,[23] and Gurova et al.[24]). We believe that these differences can be explained by three factors. First, we have used a rapid perturbation system and have investigated the impact of FACT loss after a depletion time of only 1 and 4 h. This is especially important when studying a multifaceted protein like FACT because it is possible that the requirement for FACT to modulate transcription through chromatin is difficult to detect in a context in which

Please cite this article in press as: Žumer et al., FACT maintains chromatin architecture and thereby stimulates RNA polymerase II pausing during transcription *in vivo*, Molecular Cell (2024), https://doi.org/10.1016/j.molcel.2024.05.003

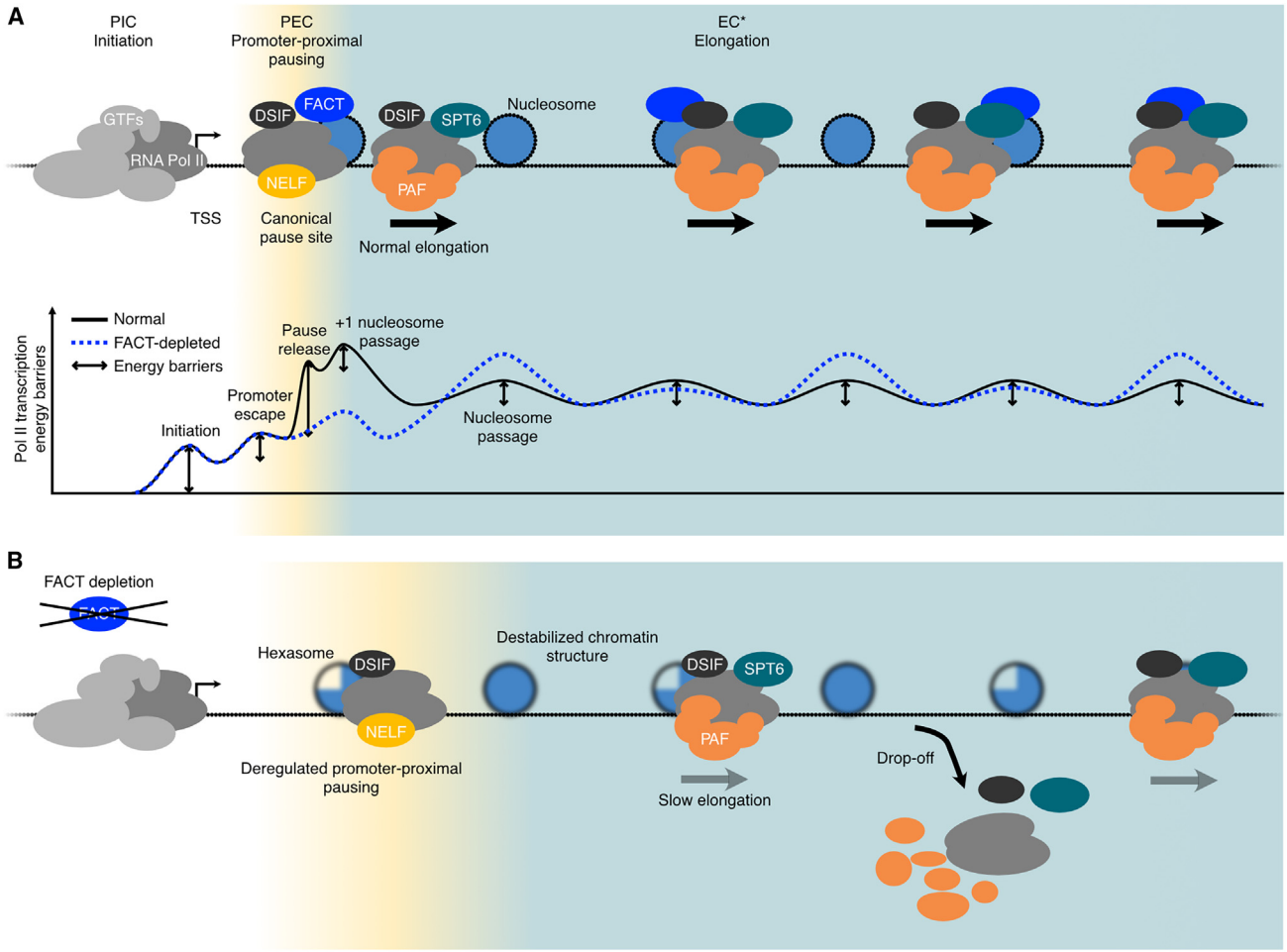

Figure 6. Model summary of the effect of FACT loss on RNA Pol II transcription

(A) Schematic representation of RNA Pol II complexes of promoter-proximal transcription and a visual representation of the energy barriers of transcription by RNA Pol II. The shading represents transcription cycle phases and corresponding RNA Pol II complexes: pre-initiation complex (PIC, white), paused-elongation complex (PEC, yellow), and activated elongation complex (EC*, teal).

(B) Schematic summary of the effect of FACT depletion on transcription.

chromatin structure has been severely perturbed due to long-term loss of FACT. Second, we used a combination of highly sensitive methods to measure nascent RNA rather than steady-state RNA, which enabled us to directly measure the synthesis of RNA instead of its accumulation in the cell. Third, we used spike-ins for data normalization, which is critical for accurate data analysis, since data normalization based on read counts can obscure the global reduction in transcription that results from loss of FACT.

To deconvolute the complex transcriptional defect that results from FACT depletion *in vivo*, we integrated biochemical *in vitro* transcription assays in our study. These experiments suggest that NELF stabilizes RNA Pol II pausing at the nucleosome border, which is consistent with a previous study that has shown that NELF depletion leads to a reduction in RNA Pol II occupancy at the pause site just upstream of the nucleosome border.[60] Notably, our *in vivo* data suggest that FACT is a pausing factor. However, our biochemical experiments clearly indicate that FACT does not function mechanistically as a pausing factor, since we did not observe an increase in pausing when FACT is included in the *in vitro* transcription assays. Of note, a previous study reported a pausing defect in *Drosophila* S2 cells after FACT knockdown and ascribed the defect to loss of histone modifications associated with active transcription.[38] However, because this study was based on long-term FACT perturbation, it is likely that these observations are secondary to the cumulative loss of chromatin structure in the absence of FACT.

Based on our data, recent work by others, and the assumptions that the exchange of RNA Pol II-bound factors and each encounter between early ECs and a nucleosome represent an energy barrier for transcription, we propose a new mechanistic model for the early elongation stages of RNA Pol II transcription (Figure 6A). In this model, NELF is recruited to the RNA Pol II complex early upon promoter escape and throttles RNA Pol II down. However, NELF alone is not sufficient to halt the transcribing RNA Pol II. It therefore needs an additional barrier,

the +1 nucleosome, to induce RNA Pol II pausing. At the same time, the effect of NELF binding on elongation speed effectively increases the barrier that the +1 nucleosome poses for productive elongation. In this model, promoter-proximal pausing is therefore dependent on cooperativity between NELF and the nucleosome barrier, whereas the pause position is determined by the position of the +1 nucleosome. Based on the relative positioning of pause sites and nucleosomes, a functional relationship between the +1 nucleosome and promoter-proximal pausing has been suggested previously.[4] Depletion of FACT has provided us with a powerful perturbation to prove this model since it allows for destabilization of nucleosomes without affecting RNA Pol II complexes directly. This separation of function *in vivo*, in combination with our *in vitro* experiments, has enabled us to provide direct evidence for the requirement of an intact +1 nucleosome to establish effective promoter-proximal pausing of RNA Pol II. This likely acts in concert with other regulators of pausing, such as DNA sequence[4] and histone modifications.[61] The proposed delay in elongation factor recruitment in the absence of FACT is based on the mutual exclusiveness of NELF and PAF[62] (Figure 6B).

In summary, by combining highly sensitive *in vivo* genomic experiments with *in vitro* transcription assays, we demonstrate the importance of FACT for transcription of chromatin and reconcile previously inconsistent observations of *in vivo* and *in vitro* studies. We show that FACT facilitates the passage of RNA Pol II through nucleosomes while also mediating retention of complete nucleosomes in the wake of transcribing RNA Pol II molecules. FACT thereby stabilizes the chromatin structure near the TSS, including +1 nucleosome integrity. This, in turn, regulates promoter-proximal pausing in subsequent transcription cycles. By facilitating nucleosome passage, FACT also supports transcription elongation and prevents premature termination. Taken together, our work provides important mechanistic insight into the seemingly contradictory role of FACT in maintaining chromatin structure and regulating transcription through nucleosomes, as well as into the general interplay between chromatin structure and transcription.

Limitations of the study

Most of our conclusions are based on experiments using rapid dTAG-mediated depletion of SSRP1 in the K562 cell line, which is a human-immortalized myelogenous leukemia cell line. The dTAG7 ligand that we used to induce SSRP1 depletion was dissolved in DMSO. We controlled for potential secondary effects of DMSO by comparing the samples that were treated with the dTAG7 ligand to samples that were treated with DMSO for the same duration. Although protein depletion with the dTAG system is fast, we cannot entirely exclude secondary effects on chromatin structure and transcription. In addition, we cannot rule out redundancy with or compensation by other proteins (e.g., chromatin remodelers) that may mask the role of FACT in chromatin architecture and transcription. It is also possible that FACT depletion leads to changes in CTCF and/or cohesin occupancy that may influence chromatin architecture. Furthermore, it is important to note that histone modifications may affect the function of FACT[63] and that the effects of FACT depletion may differ across cell types.

MNase-seq and 5′ cap-seq are dependent on enzymatic reactions for DNA digestion and RNA decapping, respectively, that may be affected by possible sequence biases of the enzymes. In addition, it is possible that deeper sequencing of the MNase-seq libraries would uncover further details with respect to the role of FACT in nucleosome architecture. Residual contamination in TT-seq libraries with unlabeled RNA cannot be entirely excluded, despite stringent washes during the procedure. mNET-seq involves immunoprecipitation with an anti-RNA-Pol-II C-terminal domain (CTD) antibody that may bind differently depending on the CTD phosphorylation status. The resolution of ChIP-seq and differences in IP efficiency preclude direct comparisons of different ChIPs and conclusions on positional differences between factors for positions that are closer than the mean length of ChIP-ed DNA fragments. For most assays, we used ectopic spike-ins to allow for detection of global changes in transcription and occupancy, but we cannot exclude minor normalization biases due to cell counting or pipetting errors that may influence the spike-in scaling factors. Finally, elongation velocity analyses are limited by the assumption that TT-seq captures output of elongating RNA Pol II, which does not hold in regions of high drop-off.

STAR★METHODS

Detailed methods are provided in the online version of this paper and include the following:

- KEY RESOURCES TABLE
- RESOURCE AVAILABILITY
  - Lead contact
  - Materials availability
  - Data and code availability
- EXPERIMENTAL MODEL AND STUDY PARTICIPANT DETAILS
  - Cell lines and cell culture
  - Proteins and nucleic acid for in vitro RNA elongation assays
- METHOD DETAILS
  - Genome editing with CRIPSR/Cas9
  - In vitro RNA elongation assays
  - Western Blotting
  - TT-seq
  - mNET-seq
  - MNase-seq
  - 5'cap-seq
  - ChIP-seq
  - Tiled-MCC
- QUANTIFICATION AND STATISTICAL ANALYSIS
  - Sequencing data preprocessing
  - Differential gene expression analyses
  - Estimation of elongation velocity
  - Metagene profiles and heatmaps
  - Determination of transcription start sites (TSS), pause sites and +1 nucleosome positions
  - Quantification of subnucleosomal fragments
  - Estimation of intragenic drop-off probability p
  - Quantification of in vitro RNA elongation assay products and barrier indexes
  - Replicates and statistics

SUPPLEMENTAL INFORMATION

Supplemental information can be found online at https://doi.org/10.1016/j.molcel.2024.05.003.

Please cite this article in press as: Žumer et al., FACT maintains chromatin architecture and thereby stimulates RNA polymerase II pausing during transcription *in vivo*, Molecular Cell (2024), https://doi.org/10.1016/j.molcel.2024.05.003

ACKNOWLEDGMENTS

We would like to thank Christiane Oberthür and Myriam Rohm for experimental support and Björn Schwalb for support with mathematical modeling of RNA Pol II drop-off. We are grateful to members of the Cramer laboratory for insightful discussions and critical reading of the manuscript. A.M.O. was supported by the Max Planck Society and the Deutsche Forschungsgemeinschaft (DFG). P.C. was supported by the Max Planck Society.

AUTHOR CONTRIBUTIONS

K.Ž. conceived and planned the study, performed experiments, bioinformatics analysis, and interpreted data; M.O. purified proteins and nucleic acids, designed and performed *in vitro* transcription experiments with U.N.; A.A. and A.M.O. designed Tiled-MCC experiments, A.A. performed and analyzed the experiments and was supervised by A.M.O.; A.Z. performed ChIP-seq experiments; A.D. designed and performed mathematical modeling of RNA Pol II drop-off; K.C.M., P.R. generated the dTAG-SSRP1 cell line, and performed TT-seq experiments; P.C. and A.M.O. acquired funding; P.C. supervised the study; K.Ž. and A.M.O. wrote the original manuscript draft; K.Ž., A.M.O., and P.C. edited the manuscript, with input from all authors. M.O., A.A., and A.Z. contributed equally and have the right to list their names first in their CV.

DECLARATION OF INTERESTS

The authors declare no competing interests.

Received: October 30, 2023
Revised: March 6, 2024
Accepted: May 2, 2024
Published: May 28, 2024

REFERENCES

1. Luger, K., Mäder, A.W., Richmond, R.K., Sargent, D.F., and Richmond, T.J. (1997). Crystal structure of the nucleosome core particle at 2.8 Å resolution. Nature *389*, 251–260. https://doi.org/10.1038/38444.
2. Yamaguchi, Y., Takagi, T., Wada, T., Yano, K., Furuya, A., Sugimoto, S., Hasegawa, J., and Handa, H. (1999). NELF, a Multisubunit Complex Containing RD, Cooperates with DSIF to Repress RNA Polymerase II Elongation. Cell *97*, 41–51. https://doi.org/10.1016/s0092-8674(00)80713-8.
3. Wada, T., Takagi, T., Yamaguchi, Y., Ferdous, A., Imai, T., Hirose, S., Sugimoto, S., Yano, K., Hartzog, G.A., Winston, F., et al. (1998). DSIF, a novel transcription elongation factor that regulates RNA polymerase II processivity, is composed of human Spt4 and Spt5 homologs. Genes Dev. *12*, 343–356.
4. Core, L., and Adelman, K. (2019). Promoter-proximal pausing of RNA polymerase II: a nexus of gene regulation. Genes Dev. *33*, 960–982. https://doi.org/10.1101/gad.325142.119.
5. Adelman, K., and Lis, J.T. (2012). Promoter-proximal pausing of RNA polymerase II: emerging roles in metazoans. Nat. Rev. Genet. *13*, 720–731. https://doi.org/10.1038/nrg3293.
6. Orphanides, G., LeRoy, G., Chang, C.H., Luse, D.S., and Reinberg, D. (1998). FACT, a Factor that Facilitates Transcript Elongation through Nucleosomes. Cell *92*, 105–116. https://doi.org/10.1016/s0092-8674(00)80903-4.
7. Orphanides, G., Wu, W.H., Lane, W.S., Hampsey, M., and Reinberg, D. (1999). The chromatin-specific transcription elongation factor FACT comprises human SPT16 and SSRP1 proteins. Nature *400*, 284–288. https://doi.org/10.1038/22350.
8. Wittmeyer, J., and Formosa, T. (1997). The Saccharomyces cerevisiae DNA Polymerase α Catalytic Subunit Interacts with Cdc68/Spt16 and with Pob3, a Protein Similar to an HMG1-Like Protein. Mol. Cell. Biol. *17*, 4178–4190. https://doi.org/10.1128/MCB.17.7.4178.
9. Winkler, D.D., and Luger, K. (2011). The Histone Chaperone FACT: Structural Insights and Mechanisms for Nucleosome Reorganization. J. Biol. Chem. *286*, 18369–18374. https://doi.org/10.1074/jbc.R110.180778.
10. Liu, Y., Zhou, K., Zhang, N., Wei, H., Tan, Y.Z., Zhang, Z., Carragher, B., Potter, C.S., D'Arcy, S., and Luger, K. (2020). FACT caught in the act of manipulating the nucleosome. Nature *577*, 426–431. https://doi.org/10.1038/s41586-019-1820-0.
11. Jeronimo, C., Angel, A., Nguyen, V.Q., Kim, J.M., Poitras, C., Lambert, E., Collin, P., Mellor, J., Wu, C., and Robert, F. (2021). FACT is recruited to the +1 nucleosome of transcribed genes and spreads in a Chd1-dependent manner. Mol. Cell *81*, 3542–3559.e11. https://doi.org/10.1016/j.molcel.2021.07.010.
12. Martin, B.J.E., Chruscicki, A.T., and Howe, L.J. (2018). Transcription Promotes the Interaction of the FAcilitates Chromatin Transactions (FACT) Complex with Nucleosomes in Saccharomyces cerevisiae. Genetics *210*, 869–881. https://doi.org/10.1534/genetics.118.301349.
13. Farnung, L., Ochmann, M., Engeholm, M., and Cramer, P. (2021). Structural basis of nucleosome transcription mediated by Chd1 and FACT. Nat. Struct. Mol. Biol. *28*, 382–387. https://doi.org/10.1038/s41594-021-00578-6.
14. Ehara, H., Kujirai, T., Shirouzu, M., Kurumizaka, H., and Sekine, S.-I. (2022). Structural basis of nucleosome disassembly and reassembly by RNAPII elongation complex with FACT. Science *377*, eabp9466. https://doi.org/10.1126/science.abp9466.
15. Tsunaka, Y., Fujiwara, Y., Oyama, T., Hirose, S., and Morikawa, K. (2016). Integrated molecular mechanism directing nucleosome reorganization by human FACT. Genes Dev. *30*, 673–686.
16. Wang, T., Liu, Y., Edwards, G., Krzizike, D., Scherman, H., and Luger, K. (2018). The histone chaperone FACT modulates nucleosome structure by tethering its components. Life Sci. Alliance *1*, e201800107. https://doi.org/10.26508/lsa.201800107.
17. Belotserkovskaya, R., Oh, S., Bondarenko, V.A., Orphanides, G., Studitsky, V.M., and Reinberg, D. (2003). FACT facilitates transcription-dependent nucleosome alteration. Science *301*, 1090–1093. https://doi.org/10.1126/science.1085703.
18. Chen, P., Dong, L., Hu, M., Wang, Y.Z., Xiao, X., Zhao, Z., Yan, J., Wang, P.Y., Reinberg, D., Li, M., et al. (2018). Functions of FACT in Breaking the Nucleosome and Maintaining Its Integrity at the Single-Nucleosome Level. Mol. Cell *71*, 284–293.e4. https://doi.org/10.1016/j.molcel.2018.06.020.
19. Hsieh, F.-K., Kulaeva, O.I., Patel, S.S., Dyer, P.N., Luger, K., Reinberg, D., and Studitsky, V.M. (2013). Histone chaperone FACT action during transcription through chromatin by RNA polymerase II. Proc. Natl. Acad. Sci. USA *110*, 7654–7659. https://doi.org/10.1073/pnas.1222198110.
20. Pavri, R., Zhu, B., Li, G., Trojer, P., Mandal, S., Shilatifard, A., and Reinberg, D. (2006). Histone H2B Monoubiquitination Functions Cooperatively with FACT to Regulate Elongation by RNA Polymerase II. Cell *125*, 703–717. https://doi.org/10.1016/j.cell.2006.04.029.
21. Zhou, K., Liu, Y., and Luger, K. (2020). Histone chaperone FACT FAcilitates Chromatin Transcription: mechanistic and structural insights. Curr. Opin. Struct. Biol. *65*, 26–32. https://doi.org/10.1016/j.sbi.2020.05.019.
22. Formosa, T., and Winston, F. (2020). The role of FACT in managing chromatin: disruption, assembly, or repair? Nucleic Acids Res. *48*, 11929–11941. https://doi.org/10.1093/nar/gkaa912.
23. Jeronimo, C., and Robert, F. (2022). The histone chaperone FACT: a guardian of chromatin structure integrity. Transcription *13*, 16–38. https://doi.org/10.1080/21541264.2022.2069995.
24. Gurova, K., Chang, H.-W., Valieva, M.E., Sandlesh, P., and Studitsky, V.M. (2018). Structure and function of the histone chaperone FACT – Resolving

Please cite this article in press as: Žumer et al., FACT maintains chromatin architecture and thereby stimulates RNA polymerase II pausing during transcription *in vivo*, Molecular Cell (2024), https://doi.org/10.1016/j.molcel.2024.05.003

FACTual issues. Biochim. Biophys. Acta Gene Regul. Mech. *1861*, 892–904. https://doi.org/10.1016/j.bbagrm.2018.07.008.

25. Mylonas, C., and Tessarz, P. (2018). Transcriptional repression by FACT is linked to regulation of chromatin accessibility at the promoter of ES cells. Life Sci. Alliance *1*, e201800085. https://doi.org/10.26508/lsa.201800085.
26. True, J.D., Muldoon, J.J., Carver, M.N., Poorey, K., Shetty, S.J., Bekiranov, S., and Auble, D.T. (2016). The Modifier of Transcription 1 (Mot1) ATPase and Spt16 Histone Chaperone Co-regulate Transcription through Preinitiation Complex Assembly and Nucleosome Organization. J. Biol. Chem. *291*, 15307–15319. https://doi.org/10.1074/jbc.M116.735134.
27. Chen, F., Zhang, W., Xie, D., Gao, T., Dong, Z., and Lu, X. (2020). Histone chaperone FACT represses retrotransposon MERVL and MERVL-derived cryptic promoters. Nucleic Acids Res. *48*, 10211–10225. https://doi.org/10.1093/nar/gkaa732.
28. Biswas, D., Dutta-Biswas, R., Mitra, D., Shibata, Y., Strahl, B.D., Formosa, T., and Stillman, D.J. (2006). Opposing roles for Set2 and yFACT in regulating TBP binding at promoters. EMBO J. *25*, 4479–4489. https://doi.org/10.1038/sj.emboj.7601333.
29. Li, Y., Zeng, S.X., Landais, I., and Lu, H. (2007). Human SSRP1 Has Spt16-dependent and -independent Roles in Gene Transcription. J. Biol. Chem. *282*, 6936–6945. https://doi.org/10.1074/jbc.M603822200.
30. Fleyshman, D., Prendergast, L., Safina, A., Paszkiewicz, G., Commane, M., Morgan, K., Attwood, K., and Gurova, K. (2017). Level of FACT defines the transcriptional landscape and aggressive phenotype of breast cancer cells. Oncotarget *8*, 20525–20542. https://doi.org/10.18632/oncotarget.15656.
31. Sandlesh, P., Safina, A., Goswami, I., Prendergast, L., Rosario, S., Gomez, E.C., Wang, J., and Gurova, K.V. (2020). Prevention of Chromatin Destabilization by FACT Is Crucial for Malignant Transformation. iScience *23*, 101177. https://doi.org/10.1016/j.isci.2020.101177.
32. Voth, W.P., Takahata, S., Nishikawa, J.L., Metcalfe, B.M., Näär, A.M., and Stillman, D.J. (2014). A Role for FACT in Repopulation of Nucleosomes at Inducible Genes. PLoS One *9*, e84092. https://doi.org/10.1371/journal.pone.0084092.
33. Hossan, T., Nagarajan, S., Baumgart, S.J., Xie, W., Magallanes, R.T., Hernandez, C., Chiaroni, P.M., Indenbirken, D., Spitzner, M., Thomas-Chollier, M., et al. (2016). Histone Chaperone SSRP1 is Essential for Wnt Signaling Pathway Activity During Osteoblast Differentiation. Stem Cells *34*, 1369–1376. https://doi.org/10.1002/stem.2287.
34. Cheung, V., Chua, G., Batada, N.N., Landry, C.R., Michnick, S.W., Hughes, T.R., and Winston, F. (2008). Chromatin- and Transcription-Related Factors Repress Transcription from within Coding Regions throughout the Saccharomyces cerevisiae Genome. PLoS Biol. *6*, e277. https://doi.org/10.1371/journal.pbio.0060277.
35. Mason, P.B., and Struhl, K. (2003). The FACT Complex Travels with Elongating RNA Polymerase II and Is Important for the Fidelity of Transcriptional Initiation In Vivo. Mol. Cell. Biol. *23*, 8323–8333. https://doi.org/10.1128/MCB.23.22.8323-8333.2003.
36. Kaplan, C.D., Laprade, L., and Winston, F. (2003). Transcription Elongation Factors Repress Transcription Initiation from Cryptic Sites. Science *301*, 1096–1099. https://doi.org/10.1126/science.1087374.
37. Jeronimo, C., Watanabe, S., Kaplan, C.D., Peterson, C.L., and Robert, F. (2015). The Histone Chaperones FACT and Spt6 Restrict H2A. Mol. Cell *58*, 1113–1123. https://doi.org/10.1016/j.molcel.2015.03.030.
38. Tettey, T.T., Gao, X., Shao, W., Li, H., Story, B.A., Chitsazan, A.D., Glaser, R.L., Goode, Z.H., Seidel, C.W., Conaway, R.C., et al. (2019). A Role for FACT in RNA Polymerase II Promoter-Proximal Pausing. Cell Rep. *27*, 3770–3779.e7. https://doi.org/10.1016/j.celrep.2019.05.099.
39. Jamai, A., Puglisi, A., and Strubin, M. (2009). Histone Chaperone Spt16 Promotes Redeposition of the Original H3-H4 Histones Evicted by Elongating RNA Polymerase. Mol. Cell *35*, 377–383. https://doi.org/10.1016/j.molcel.2009.07.001.
40. Schwabish, M.A., and Struhl, K. (2004). Evidence for Eviction and Rapid Deposition of Histones upon Transcriptional Elongation by RNA Polymerase II. Mol. Cell. Biol. *24*, 10111–10117. https://doi.org/10.1128/MCB.24.23.10111-10117.2004.
41. Jeronimo, C., Poitras, C., and Robert, F. (2019). Histone Recycling by FACT and Spt6 during Transcription Prevents the Scrambling of Histone Modifications. Cell Rep. *28*, 1206–1218.e8. https://doi.org/10.1016/j.celrep.2019.06.097.
42. Goswami, I., Sandlesh, P., Stablewski, A., Toshkov, I., Safina, A.F., Magnitov, M., Wang, J., and Gurova, K. (2022). FACT maintains nucleosomes during transcription and stem cell viability in adult mice. EMBO Rep. *23*, e53684. https://doi.org/10.15252/embr.202153684.
43. Nabet, B., Roberts, J.M., Buckley, D.L., Paulk, J., Dastjerdi, S., Yang, A., Leggett, A.L., Erb, M.A., Lawlor, M.A., Souza, A., et al. (2018). The dTAG system for immediate and target-specific protein degradation. Nat. Chem. Biol. *14*, 431–441. https://doi.org/10.1038/s41589-018-0021-8.
44. Chen, K., Xi, Y., Pan, X., Li, Z., Kaestner, K., Tyler, J., Dent, S., He, X., and Li, W. (2013). DANPOS: Dynamic analysis of nucleosome position and occupancy by sequencing. Genome Res. *23*, 341–351.
45. Ramachandran, S., Ahmad, K., and Henikoff, S. (2017). Transcription and Remodeling Produce Asymmetrically Unwrapped Nucleosomal Intermediates. Mol. Cell *68*, 1038–1053.e4. https://doi.org/10.1016/j.molcel.2017.11.015.
46. Fu, Y., Sinha, M., Peterson, C.L., and Weng, Z. (2008). The Insulator Binding Protein CTCF Positions 20 Nucleosomes around Its Binding Sites across the Human Genome. PLoS Genet. *4*, e1000138. https://doi.org/10.1371/journal.pgen.1000138.
47. Barisic, D., Stadler, M.B., Iurlaro, M., and Schübeler, D. (2019). Mammalian ISWI and SWI/SNF selectively mediate binding of distinct transcription factors. Nature *569*, 136–140. https://doi.org/10.1038/s41586-019-1115-5.
48. Mirny, L.A., Imakaev, M., and Abdennur, N. (2019). Two major mechanisms of chromosome organization. Curr. Opin. Cell Biol. *58*, 142–152. https://doi.org/10.1016/j.ceb.2019.05.001.
49. Aljahani, A., Hua, P., Karpinska, M.A., Quililan, K., Davies, J.O.J., and Oudelaar, A.M. (2022). Analysis of sub-kilobase chromatin topology reveals nano-scale regulatory interactions with variable dependence on cohesin and CTCF. Nat. Commun. *13*, 2139. https://doi.org/10.1038/s41467-022-29696-5.
50. Cao, F., Fang, Y., Tan, H.K., Goh, Y., Choy, J.Y.H., Koh, B.T.H., Hao Tan, J., Bertin, N., Ramadass, A., Hunter, E., et al. (2017). Super-Enhancers and Broad H3K4me3 Domains Form Complex Gene Regulatory Circuits Involving Chromatin Interactions. Sci. Rep. *7*, 2186. https://doi.org/10.1038/s41598-017-02257-3.
51. Krietenstein, N., Abraham, S., Venev, S.V., Abdennur, N., Gibcus, J., Hsieh, T.S., Parsi, K.M., Yang, L., Maehr, R., Mirny, L.A., et al. (2020). Ultrastructural Details of Mammalian Chromosome Architecture. Mol. Cell *78*, 554–565.e7. https://doi.org/10.1016/j.molcel.2020.03.003.
52. Crump, N.T., Smith, A.L., Godfrey, L., Dopico-Fernandez, A.M., Denny, N., Harman, J.R., Hamley, J.C., Jackson, N.E., Chahrour, C., Riva, S., et al. (2023). MLL-AF4 cooperates with PAF1 and FACT to drive high-density enhancer interactions in leukemia. Nat. Commun. *14*, 5208. https://doi.org/10.1038/s41467-023-40981-9.
53. Schwalb, B., Michel, M., Zacher, B., Frühauf, K., Demel, C., Tresch, A., Gagneur, J., and Cramer, P. (2016). TT-seq maps the human transient transcriptome. Science *352*, 1225–1228. https://doi.org/10.1126/science.aad9841.
54. Klein, D.C., Lardo, S.M., McCannell, K.N., and Hainer, S.J. (2023). FACT regulates pluripotency through proximal and distal regulation of gene expression in murine embryonic stem cells. BMC Biol. *21*, 167. https://doi.org/10.1186/s12915-023-01669-0.
55. Žumer, K., Maier, K.C., Farnung, L., Jaeger, M.G., Rus, P., Winter, G., and Cramer, P. (2021). Two distinct mechanisms of RNA polymerase II

Please cite this article in press as: Žumer et al., FACT maintains chromatin architecture and thereby stimulates RNA polymerase II pausing during transcription *in vivo*, Molecular Cell (2024), https://doi.org/10.1016/j.molcel.2024.05.003

elongation stimulation in vivo. Mol. Cell *81*, 3096–3109.e8. https://doi.org/10.1016/j.molcel.2021.05.028.

56. Nojima, T., Gomes, T., Grosso, A.R.F., Kimura, H., Dye, M.J., Dhir, S., Carmo-Fonseca, M., and Proudfoot, N.J. (2015). Mammalian NET-Seq Reveals Genome-wide Nascent Transcription Coupled to RNA Processing. Cell *161*, 526–540. https://doi.org/10.1016/j.cell.2015.03.027.
57. Caizzi, L., Monteiro-Martins, S., Schwalb, B., Lysakovskaia, K., Schmitzova, J., Sawicka, A., Chen, Y., Lidschreiber, M., and Cramer, P. (2021). Efficient RNA polymerase II pause release requires U2 snRNP function. Mol. Cell *81*, 1920–1934.e9. https://doi.org/10.1016/j.molcel.2021.02.016.
58. Vos, S.M., Farnung, L., Urlaub, H., and Cramer, P. (2018). Structure of paused transcription complex Pol II–DSIF–NELF. Nature *560*, 601–606. https://doi.org/10.1038/s41586-018-0442-2.
59. Farnung, L., Ochmann, M., Garg, G., Vos, S.M., and Cramer, P. (2022). Structure of a backtracked hexasomal intermediate of nucleosome transcription. Mol. Cell *82*, 3126–3134.e7. https://doi.org/10.1016/j.molcel.2022.06.027.
60. Aoi, Y., Smith, E.R., Shah, A.P., Rendleman, E.J., Marshall, S.A., Woodfin, A.R., Chen, F.X., Shiekhattar, R., and Shilatifard, A. (2020). NELF Regulates a Promoter-Proximal Step Distinct from RNA Pol II Pause-Release. Mol. Cell *78*, 261–274.e5. https://doi.org/10.1016/j.molcel.2020.02.014.
61. Wang, H., Fan, Z., Shliaha, P.V., Miele, M., Hendrickson, R.C., Jiang, X., and Helin, K. (2023). H3K4me3 regulates RNA polymerase II promoter-proximal pause-release. Nature *615*, 339–348. https://doi.org/10.1038/s41586-023-05780-8.
62. Vos, S.M., Farnung, L., Boehning, M., Wigge, C., Linden, A., Urlaub, H., and Cramer, P. (2018). Structure of activated transcription complex Pol II–DSIF–PAF–SPT6. Nature *560*, 607–612. https://doi.org/10.1038/s41586-018-0440-4.
63. Luo, A., Kong, J., Chen, J., Xiao, X., Lan, J., Li, X., Liu, C., Wang, P.Y., Li, G., Li, W., et al. (2023). H2B ubiquitination recruits FACT to maintain a stable altered nucleosome state for transcriptional activation. Nat. Commun. *14*, 741. https://doi.org/10.1038/s41467-023-36467-3.
64. Kundaje, A., Kyriazopoulou-Panagiotopoulou, S., Libbrecht, M., Smith, C.L., Raha, D., Winters, E.E., Johnson, S.M., Snyder, M., Batzoglou, S., Sidow, A., et al. (2012). Ubiquitous heterogeneity and asymmetry of the chromatin environment at regulatory elements. Genome Res. *22*, 1735–1747. https://doi.org/10.1101/gr.136366.111.
65. Dodonova, S.O., Zhu, F., Dienemann, C., Taipale, J., and Cramer, P. (2020). Nucleosome-bound SOX2 and SOX11 structures elucidate pioneer factor function. Nature *580*, 669–672. https://doi.org/10.1038/s41586-020-2195-y.
66. Farnung, L., Vos, S.M., Wigge, C., and Cramer, P. (2017). Nucleosome-Chd1 structure and implications for chromatin remodelling. Nature *550*, 539–542. https://doi.org/10.1038/nature24046.
67. Bernecky, C., Plitzko, J.M., and Cramer, P. (2017). Structure of a transcribing RNA polymerase II-DSIF complex reveals a multidentate DNA-RNA clamp. Nat. Struct. Mol. Biol. *24*, 809–815. https://doi.org/10.1038/nsmb.3465.
68. Schindelin, J., Arganda-Carreras, I., Frise, E., Kaynig, V., Longair, M., Pietzsch, T., Preibisch, S., Rueden, C., Saalfeld, S., Schmid, B., et al. (2012). Fiji: an open-source platform for biological-image analysis. Nat. Methods *9*, 676–682. https://doi.org/10.1038/nmeth.2019.
69. Swift, M.L., and GraphPad Prism. (1997). Data Analysis, and Scientific Graphing. J. Chem. Inf. Comput. Sci. *37*, 411–412. https://doi.org/10.1021/ci960402j.
70. R Core Team (2021). R: A language and environment for statistical computing (Vienna, Austria: R Foundation for Statistical Computing). https://www.R-project.org/.
71. RStudio Team (2020). RStudio: Integrated Development for R. RStudio (Boston, MA: PBC). http://www.rstudio.com/.
72. Gentleman, R.C., Carey, V.J., Bates, D.M., Bolstad, B., Dettling, M., Dudoit, S., Ellis, B., Gautier, L., Ge, Y., Gentry, J., et al. (2004). Bioconductor: open software development for computational biology and bioinformatics. Genome Biol. *5*, R80. https://doi.org/10.1186/gb-2004-5-10-r80.
73. Huber, W., Carey, V.J., Gentleman, R., Anders, S., Carlson, M., Carvalho, B.S., Bravo, H.C., Davis, S., Gatto, L., Girke, T., et al. (2015). Orchestrating high-throughput genomic analysis with Bioconductor. Nat. Methods *12*, 115–121. https://doi.org/10.1038/nmeth.3252.
74. Martin, M. (2011). Cutadapt removes adapter sequences from high-throughput sequencing reads. EMBnet. j. *17*, 3. https://doi.org/10.14806/ej.17.1.200.
75. Dobin, A., Davis, C.A., Schlesinger, F., Drenkow, J., Zaleski, C., Jha, S., Batut, P., Chaisson, M., and Gingeras, T.R. (2013). STAR: ultrafast universal RNA-seq aligner. Bioinformatics *29*, 15–21. https://doi.org/10.1093/bioinformatics/bts635.
76. Wickham, H., Averick, M., Bryan, J., Chang, W., McGowan, L., François, R., Grolemund, G., Hayes, A., Henry, L., Hester, J., et al. (2019). Welcome to the Tidyverse. J. Open Source Software *4*, 1686. https://doi.org/10.21105/joss.01686.
77. Smith, T., Heger, A., and Sudbery, I. (2017). UMI-tools: modeling sequencing errors in Unique Molecular Identifiers to improve quantification accuracy. Genome Res. *27*, 491–499.
78. Langmead, B., and Salzberg, S.L. (2012). Fast gapped-read alignment with Bowtie 2. Nat. Methods *9*, 357–359. https://doi.org/10.1038/nmeth.1923.
79. Dyer, P.N., Edayathumangalam, R.S., White, C.L., Bao, Y., Chakravarthy, S., Muthurajan, U.M., and Luger, K. (2004). Reconstitution of nucleosome core particles from recombinant histones and DNA. In Methods in Enzymology, *375* (Academic Press), pp. 23–44.
80. Levendosky, R.F., Sabantsev, A., Deindl, S., and Bowman, G.D. (2016). The Chd1 chromatin remodeler shifts hexasomes unidirectionally. eLife *5*, e21356. https://doi.org/10.7554/eLife.21356.
81. Farnung, L., Vos, S.M., and Cramer, P. (2018). Structure of transcribing RNA polymerase II-nucleosome complex. Nat. Commun. *9*, 5432. https://doi.org/10.1038/s41467-018-07870-y.
82. Żylicz, J.J., Bousard, A., Žumer, K., Dossin, F., Mohammad, E., da Rocha, S.T., Schwalb, B., Syx, L., Dingli, F., Loew, D., et al. (2019). The Implication of Early Chromatin Changes in X Chromosome Inactivation. Cell *176*, 182–197.e23. https://doi.org/10.1016/j.cell.2018.11.041.
83. Schlackow, M., Nojima, T., Gomes, T., Dhir, A., Carmo-Fonseca, M., and Proudfoot, N.J. (2017). Distinctive Patterns of Transcription and RNA Processing for Human lincRNAs. Mol. Cell *65*, 25–38. https://doi.org/10.1016/j.molcel.2016.11.029.
84. Adjalley, S.H., Chabbert, C.D., Klaus, B., Pelechano, V., and Steinmetz, L.M. (2016). Landscape and Dynamics of Transcription Initiation in the Malaria Parasite Plasmodium falciparum. Cell Rep. *14*, 2463–2475. https://doi.org/10.1016/j.celrep.2016.02.025.
85. Pelechano, V., Wei, W., and Steinmetz, L.M. (2015). Widespread Co-translational RNA Decay Reveals Ribosome Dynamics. Cell *161*, 1400–1412. https://doi.org/10.1016/j.cell.2015.05.008.
86. Oudelaar, A.M., Beagrie, R.A., Gosden, M., de Ornellas, S., Georgiades, E., Kerry, J., Hidalgo, D., Carrelha, J., Shivalingam, A., El-Sagheer, A.H., et al. (2020). Dynamics of the 4D genome during in vivo lineage specification and differentiation. Nat. Commun. *11*, 2722. https://doi.org/10.1038/s41467-020-16598-7.
87. Hua, P., Badat, M., Hanssen, L.L.P., Hentges, L.D., Crump, N., Downes, D.J., Jeziorska, D.M., Oudelaar, A.M., Schwessinger, R., Taylor, S., et al. (2021). Defining genome architecture at base-pair resolution. Nature *595*, 125–129. https://doi.org/10.1038/s41586-021-03639-4.
88. Servant, N., Varoquaux, N., Lajoie, B.R., Viara, E., Chen, C.J., Vert, J.P., Heard, E., Dekker, J., and Barillot, E. (2015). HiC-Pro: an optimized and

Please cite this article in press as: Žumer et al., FACT maintains chromatin architecture and thereby stimulates RNA polymerase II pausing during transcription *in vivo*, Molecular Cell (2024), https://doi.org/10.1016/j.molcel.2024.05.003

flexible pipeline for Hi-C data processing. Genome Biol. *16*, 259. https://doi.org/10.1186/s13059-015-0831-x.

89. Love, M.I., Huber, W., and Anders, S. (2014). Moderated estimation of fold change and dispersion for RNA-seq data with DESeq2. Genome Biol. *15*, 550. https://doi.org/10.1186/s13059-014-0550-8.

90. O'Leary, N.A., Wright, M.W., Brister, J.R., Ciufo, S., Haddad, D., McVeigh, R., Rajput, B., Robbertse, B., Smith-White, B., Ako-Adjei, D., et al. (2016). Reference sequence (RefSeq) database at NCBI: current status, taxonomic expansion, and functional annotation. Nucleic Acids Res. *44*, D733–D745. https://doi.org/10.1093/nar/gkv1189.

91. Wickham, H.W. (2016). ggplot2, Second Edition (Springer).

92. Schindelin, J., Arganda-Carreras, I., Frise, E., Kaynig, V., Longair, M., Pietzsch, T., Preibisch, S., Rueden, C., Saalfeld, S., Schmid, B., et al. (2012). Fiji: an open-source platform for biological-image analysis. Nat. Methods *9*, 676–682. https://doi.org/10.1038/nmeth.2019.

Please cite this article in press as: Žumer et al., FACT maintains chromatin architecture and thereby stimulates RNA polymerase II pausing during transcription *in vivo*, Molecular Cell (2024), https://doi.org/10.1016/j.molcel.2024.05.003

STAR★METHODS

KEY RESOURCES TABLE

REAGENT or RESOURCE	SOURCE	IDENTIFIER
Antibodies		
anti-RNA Pol II CTD (total)	Diagenode	C15200004, RRID;AB_2728744
anti-HA	Roche	11867423001; RRID:AB_390918
anti-alpha-tubulin	SCBT	sc-69971; RRID:AB_2210059
anti-H3	Abcam	ab21054; RRID:AB_880437
anti-U1-snRNP70	SCBT	sc-390899; RRID:AB_2801569
anti-SPT16	BioLegend	607008; RRID:AB_2721598
anti-SSRP1	BioLegend	609710; RRID:AB_2650944
Rpb1 NTD antibody	Cell Signaling Technology	14958; RRID:AB_2687876
Th1L (NELF C/D) antibody	Cell Signaling Technology	12265; RRID:AB_2797862
Spike-in Antibody	Active Motif	61686; RRID:AB_2737370
Bacterial and virus strains		
BL21 (RIL) DE3	Agilent	230245
XL1 Blue	Agilent	200249
Hi5 cells	Expression Systems	94-002F
Sf9 cells	Thermo Fischer	12659017
Sf21 cells	Expression Systems	94-003S
ESF 921	Expression Systems	96-001-01
Biological samples		
Sus scrofa thymus	Locally sourced	N/A
Chemicals, peptides, and recombinant proteins		
EZ-link HPDP-biotin	Pierce	21341
DMSO	Sigma-Aldrich	D8418-50ML
4-thiouridne	Carbosynth	NT06186
Empigen	Sigma-Aldrich	30326-250ML
dTAG7 ligand	Tocris	6912
T4 PNK 3' phosphatase minus	NEB	M0236
TURBO DNA-free DNAse	Thermo Fisher Scientific	AM1907
NEBNext Magnesium RNA Fragmentation Module	NEB	E6150S
T4 PNK	NEB	M0201S
Dynabeads M-280 Sheep Anti-Mouse IgG	Thermo Fisher Scientific	11201D
Superscript III	Thermo Fisher Scientific	18080-044
4 % E-Gel (HR)	Thermo Fisher Scientific	G501804
Terminator 5'-Phosphate-Dependent Exonuclease	Epicenter	TER51020
Quick CIP	NEB	M0525S
Proteinase K	Thermo Fisher Scientific	AM2546
SUPERase• In	Thermo Fisher Scientific	AM2694
NEBNext Magnesium RNA Fragmentation Module	NEB	E6150S
T4 RNA Ligase 1 (ssRNA Ligase)	NEB	M0204S
T4 DNA Ligase	NEB	M0202T
Phusion High-Fidelity PCR Master Mix with HF Buffer	NEB	M0531S
Klenow Fragment (3'-5' exo-)	NEB	M0212S
NEBNext End Repair Module	NEB	E6050S
dATP Solution	NEB	N0440S

(*Continued on next page*)

Please cite this article in press as: Žumer et al., FACT maintains chromatin architecture and thereby stimulates RNA polymerase II pausing during transcription *in vivo*, Molecular Cell (2024), https://doi.org/10.1016/j.molcel.2024.05.003

CellPress
OPEN ACCESS

Continued

REAGENT or RESOURCE	SOURCE	IDENTIFIER
Cap-Clip Acid Pyrophosphatase	CELLSCRIPT	C-CC15011H
Deoxynucleotide Solution Mix	NEB	N0447S
TURBO DNA-free Kit	Thermo Fisher Scientific	AM1907
Superscript II Reverse Transcriptase	Thermo Fisher Scientific	18064022
Random Primers	Thermo Fisher Scientific	48190011
Dynabeads M-280 Streptavidin	Thermo Fisher Scientific	11205D
Phenol:chloroform:isoamyl Alcohol 25:24:1	Sigma-Aldrich	P3803
Qiazol	Qiagen	79306
Phusion® HF Buffer	New England Biolabs	B0518S
Phusion DNA Polymerase	In house	N/A
TspRI	New England Biolabs	R0582S
NTP Set	Thermo Fischer	R0481
Micrococcal nuclease (MNase)	NEB	Cat# M0247
EGTA	Sigma-Aldrich	Cat# E3889
DNA polymerase I large (Klenow) fragment	NEB	Cat# M0210
T4 DNA ligase	Thermo Scientific	Cat# EL0013
DNA ligase buffer	Thermo Scientific	Cat# B69
dNTP mix	NEB	Cat# N0447
AMPure XP beads	Beckman Coulter	Cat# A63881
Dimethyl sulfoxide (DMSO)	Sigma-Aldrich	D2438-10ML
Formaldehyde 16% concentrate stock methanol-free	Thermo Fisher Scientific	28908
PhosSTOP	Sigma-Aldrich	4906837001
Protease Inhibitor Cocktail	Sigma-Aldrich	P8340-5ML
Dynabeads® Protein G for Immunoprecipitation	Invitrogen	10004D
Critical commercial assays		
NEBNext Ultra II DNA Library Prep Kit for Illumina	NEB	E7645S
MEGAscript T7 Transcription Kit	Thermo Fisher Scientific	AM1333
Small RNA library kit	Illumina	RS-200-0012
Illumina Stranded Total RNA Prep, Ligation kit with Ribo-Zero Plus	Illumina	20040525
Dynabeads mRNA Purification kit	Thermo Fisher Scientific	61006
Monarch kit	NEB	T1030S
miRNeasy Micro kit	Qiagen	217084
Quick-RNA microPrep + Zymo-Spin IC Columns	ZYMO	R1050 + C1004-50
μMACS Streptavidin Kit	Miltenyi	130-074-101
DNeasy blood and tissue kit	Qiagen	Cat# 69504
NEBNext ® Ultra ™ II DNA Library Prep Kit for Illumina	NEB	Cat# E7645
Twist Hybridization and Wash Kit	Twist Bioscience	Cat# 101025
Deposited data		
1 h dTAG7/DMSO control TT-seq SSRP1-dTAG K562	This study	GEO GSE242374
1 h dTAG7/DMSO control mNETseq SSRP1-dTAG K562	This study	GEO GSE242376
4 h dTAG7/DMSO control TT-seq SSRP1-dTAG K562	This study	GEO GSE242374
4 h dTAG7/DMSO control mNETseq SSRP1-dTAG K562	This study	GEO GSE242376
1 h dTAG7/DMSO control MNase-seq SSRP1-dTAG K562	This study	GEO GSE242379
1 h dTAG7/DMSO control 5cap-seq SSRP1-dTAG K562	This study	GEO GSE242378
4 h dTAG7/DMSO control MNase-seq SSRP1-dTAG K562	This study	GEO GSE242379
4 h dTAG7/DMSO control 5cap-seq SSRP1-dTAG K562	This study	GEO GSE242378
1 h dTAG7/DMSO control RNA Pol II ChIP-seq SSRP1-dTAG K562	This study	GEO GSE242380

(*Continued on next page*)

Please cite this article in press as: Žumer et al., FACT maintains chromatin architecture and thereby stimulates RNA polymerase II pausing during transcription *in vivo*, Molecular Cell (2024), https://doi.org/10.1016/j.molcel.2024.05.003

Continued

REAGENT or RESOURCE	SOURCE	IDENTIFIER
4 h dTAG7/DMSO control RNA Pol II ChIP-seq SSRP1-dTAG K562	This study	GEO GSE242380
1 h dTAG7/DMSO control Th1L ChIP-seq SSRP1-dTAG K562	This study	GEO GSE242380
4 h dTAG7/DMSO control Th1L ChIP-seq SSRP1-dTAG K562	This study	GEO GSE242380
4 h dTAG7/DMSO control Tiled-MCC	This study	GEO GSE241421
MNase-seq K562	Kundaje et al.[64]	GEO GSM920557 ENCODE
DNase I Hypersensitivity	ENCODE	GEO GSM736566
H3K27ac ChIP-seq	ENCODE	GEO GSM733656
CTCF ChIP-seq	ENCODE	GEO GSM733719
Human reference genome NCBI build 38, GRCh38	Genome Reference Consortium	http://www.ncbi.nlm.nih.gov/projects/genome/assembly/grc/human/
Experimental models: Cell lines		
K562	DSMZ	ACC 10
K562 SSRP1-dTAG clone N1C10	This study	N/A
Experimental models: Organisms/strains		
S. cerevisiae strain BY4741	Euroscarf	ACC-Y00000
D. melanogaster S2 cell line	DSMZ	ACC 130
Oligonucleotides		
Table S1	This study	N/A
Recombinant DNA		
pET1B_Hs_H2A	Dodonova et al.[65]	Internal ID: 3695
pET22b_Hs_H2B	Dodonova et al.[65]	Internal ID: 3696
pET22b _Hs_H3	Dodonova et al.[65]	Internal ID: 3697
pET3a_H4_fl	Farnung et al.[66]	Internal ID: 3323
pIDTSmartKan_OchmannConstruct_extendedRunUp_Widom601	This paper	Internal ID: 4213
438A_Hs_NHis6-TEV_NELFC_NELFA_NELFB_NELFE	Vos et al.[58]	Internal ID: 2961
pKSUMO_10xHis-3C-SPT4_SPT5	Bernecky et al.[67]	Internal ID: 2439
438C_Hs_NHis6-MBP-N10-TEV_SPT16_SSRP1_FACT	This paper	Internal ID: 3417
1C_NHis6-MBP-N10-TEV-TFIIS_H	Farnung et al.[59]	Internal ID: 3619
Software and algorithms		
ImageJ2 – Fiji (version 2.3)	Schindelin et al.[68]	https://imagej.net/software/fiji/
GraphPad Prism (version 9.3.1)	Swift[69]	https://www.graphpad.com/scientific-software/prism/
R 4.2.3	R Core Team[70]	https://www.r-project.org/
RStudio Version 2023.09.1	R Studio Team[71]	http://www.rstudio.com/
Bioconductor 3.16	Gentleman et al.[72]; Huber et al.[73]	https://www.bioconductor.org/
FastQC v0.11.5	Babraham-Institute	https://www.bioinformatics.babraham.ac.uk/projects/fastqc/
Cutadapt 1.9.1	Martin[74]	https://cutadapt.readthedocs.io/en/stable/
STAR 2.5.2b	Dobin et al.[75]	https://github.com/alexdobin/STAR
Picard 2.9.2	Broad Institute, MIT	https://broadinstitute.github.io/picard/
tidyverse (R package collection)	Wickham et al.[76]	https://www.tidyverse.org/
UMI-tools	Smith et al.[77]	https://github.com/CGATOxford/UMI-tools
Bowtie2 2.3.4.1	Langmead and Salzberg[78]	https://bowtie-bio.sourceforge.net/bowtie2/index.shtml

Molecular Cell
Article

CellPress
OPEN ACCESS

RESOURCE AVAILABILITY

Lead contact

Further information and requests for resources and reagents should be directed to and will be fulfilled by the lead contact, Kristina Žumer (kristina.zumer@mpinat.mpg.de).

Materials availability

All unique/stable reagents generated in this study are available from the lead contact with a completed Materials Transfer Agreement.

Data and code availability

- Datasets generated in this study have been deposited in NCBI's Gene Expression Omnibus database (GEO) and are accessible through GEO Series accession numbers GSE242380 and GSE241421.
- The study does not report original code.
- Any additional information required to reanalyze the data reported in this paper is available from the lead contact upon request.

EXPERIMENTAL MODEL AND STUDY PARTICIPANT DETAILS

Cell lines and cell culture

We obtained K562 cells and *D. melanogaster* S2 cells from the DSMZ-German Collection of Microorganisms and Cell Cultures GmbH. K562 cells were subcultured in RPMI medium (Thermo Fisher Scientific) supplemented with 10 % fetal bovine serum (Thermo Fisher Scientific) and 1x GlutaMax (Thermo Fisher Scientific) maintained at 37 °C and 5 % CO_2. They were maintained at densities between $1x10^5$ and $7x10^5$ cells/ml. Genome edited cell lines were cultured in the same conditions. The cells in culture were checked for mycoplasma quarterly with the PlasmoTest kit (InvivoGen) kit and are mycoplasma negative. Depletions of dTAGed proteins were performed by supplementing the growth medium with 500 nM dTAG7 ligand dissolved in DMSO or DMSO only for the control treatment for the specified times. Both treatments were at 1:20000 dilution of DMSO.

S2 cells were subcultured in Schneider's Drosophila Medium supplemented with 10 % FBS and maintained at 27°C in a non-humidified incubator.

Yeast (*S. cerevisiae*, BY4741 strain) for spike-in RNA were streaked onto a fresh plate. A single colony was used to inoculate 50 ml yeast medium (YP + 2 % glucose) and cultured overnight at 30 °C. Cells were harvested the next day when OD reached 0.8 (absorbance at 595 nm).

Proteins and nucleic acid for in vitro RNA elongation assays

H. sapiens DSIF, TFIIS, NELF and S. scrofa RNA Pol II were purified as previously described.[58] *H. sapiens* FACT (SPT16 and SSRP1) was expressed in *Trichoplusia ni* (Hi5 insect cells). Cells were collected and resuspended in lysis buffer (300 mM NaCl, 20 mM Na-HEPES, pH 7.4, 30 mM imidiazole, 10% (v/v) glycerol, 1 mM DTT, 0.284 μg ml^{-1} leupeptin, 1.37 μg ml^{-l} pepstatin A, 0.17 mg ml^{-1} PMSF and 0.33 mg ml^{-1} benzamidine), flash-frozen in liquid nitrogen and stored at −70°C. FACT was purified from 1 L of Hi5 lysate at 4°C. The cells were thawed, lysed by sonication and cleared by centrifugation and filtration through 0.8 μm syringe filters. The clarified cell lysate was applied to two 5 mL HisTrap HP columns (Cytivia) equilibrated with lysis buffer. The column was washed with 3 column volumes of lysis buffer, high salt buffer (1 M NaCl, 20 mM Na-HEPES, pH 7.4, 30 mM imidazole, 10% (v/v) glycerol, 1 mM DTT, 0.284 μg ml^{-1} leupeptin, 1.37 μg ml^{-l} pepstatin A, 0.17 mg ml^{-1} PMSF and 0.33 mg ml^{-1} benzamidine) and lysis buffer. FACT was eluted from the column with a ten-column volume gradient of nickel elution buffer (500 mM NaCl, 20 mM Na-HEPES, pH 7.4, 500 mM imidazole, 10% (v/v) glycerol, 1 mM DTT, 0.284 μg ml^{-1} leupeptin, 1.37 μg ml^{-l} pepstatin A, 0.17 mg ml^{-1} PMSF and 0.33 mg ml^{-1} benzamidine). Elution fractions were analyzed by denaturing polyacrylamide gel electrophoresis (SDS-PAGE). Fractions containing FACT were pooled, mixed with TEV protease and dialyzed against dialysis buffer (500 mM NaCl, 20 mM Na-HEPES, pH 7.4, 30 mM imidiazole, 10% (v/v) glycerol, 1 mM DTT, 0.284 μg ml^{-1} leupeptin, 1.37 μg ml^{-l} pepstatin A, 0.17 mg ml^{-1} PMSF and 0.33 mg ml^{-1} benzamidine). The dialyzed sample was diluted to 300 mM NaCl and applied to two 5 mL HisTrap HP followed by one HiTrap Q column (Cytivia). The columns were washed with one column volume of lysis buffer. The HisTrap columns were removed and the proteins were eluted from the HiTrap Q column with ten-column volume buffer with a salt gradient. Fractions containing FACT were pooled, concentrated in a 50 kDa MWCO Amicon Ultra Centrifugal Filter (Merck) and applied to HiLoad S200 16/600 pg column equilibrated with gel filtration buffer (300 mM NaCl, 20 mM Na-HEPES, pH 7.4, 10% (v/v) glycerol, 1 mM DTT). Peak fractions were assessed by SDS-PAGE analysis. FACT fractions were pooled, concentrated in a 50 kDa MWCO Amicon Ultra Centrifugal Filter (Merck), aliquoted, flash frozen in liquid nitrogen and stored at −70°C.

H. sapiens histones (H2A, H2B, H3, H4) were expressed, purified and reconstituted to an octamer, tetramer and dimer as described.[65,79,80] The template DNA for *in vitro* transcription assays containing a TspRI restriction site 52 bp upstream of the Widom 601 sequence and was amplified by PCR, as described previously.[59,81] PCR product purification by anion exchange, TspRI digest and nucleosome reconstitution were performed as described previously.[13] Hexasomes were reconstituted as described.[80]

Reconstituted hexasomes and nucleosomes were verified on a native 2% agarose gel and quantified by spectrophotometry at 280 nm based on the molar extinction coefficients of DNA and histones at this wavelength.

METHOD DETAILS

Genome editing with CRIPSR/Cas9

Cloning and endogenous knock-in of dTAG cassettes was performed as previously described.[55] See Table S1 for oligo sequences. Clones were characterized by western blot against the dTAG-HA epitope or gene-specific antibodies (see key resources table) and Sanger-sequencing of PCR amplicons surrounding the genomic integration site.

In vitro RNA elongation assays

RNA elongation assays were performed on a single DNA sequence containing the Widom 601 nucleosome positioning sequence preceded by a 52 bp sequence, where the first 15 bp of the template strand contain only A or C nucleotides (see sequence in Table S1). The DNA template was either reconstituted to a nucleosome, to a hexasome or used as linear DNA. RNA extension of a 5'-Cy5 labeled RNA primer to determine elongation products was performed as previously described.[13,59] Concentrations refer to the final concentrations in the assay. *In vitro* transcription assays with the early elongation complex (EC ± NELF ± FACT) were set up by first incubating RNA primer (480 nM) with a transcription template (240 nM) for 10 min on ice. *S. scrofa* RNA Pol II (300 nM) was added and the reactions were incubated for 10 min on ice. DSIF (600 nM), TFIIS (180 nM) and water were added. Initial transcription was started with the addition of GTP and UTP (0.5 mM each). The initial transcription reactions were incubated for 15 min at 30°C. FACT (600 nM) or buffer only was added to the stalled transcription reactions. Transcription was resumed with simultaneous addition of ATP, CTP (0.5 mM each) and NELF (0, 150, 300, 600, 3000 nM). The final reactions consisted of 10 μL at 100 mM NaCl, 20 mM Na-HEPES, pH 7.4 at 20 °C, 5 mM $MgCl_2$, 1 mM DTT, and 4% glycerol. After 60 min at 30°C, 5 μL sample from the transcription reaction was quenched with 5 μL 2x Stop buffer (6.4 M urea, 50 mM EDTA, pH 8.0, 2x TBE buffer).

Quenched RNA extension reactions were treated with 40 μg proteinase K for 30 min at 37°C followed by denaturation at 95°C for 10 min. Six microliters of sample were loaded and separated on a 12% denaturing gel (8 M urea, 1x TBE buffer, 12% acrylamide:bisacrylamide 19:1 gel, run for 42 min at 300 V in 0.5x TBE buffer) running for 42 min in 0.5x TBE buffer at 300 V. RNA products containing the fluorescent 5'-Cy5 were visualized with a Typhoon 9500 FLA imager (GE Healthcare Life Sciences).

Western Blotting

To perform whole cell Western blot analyses, we lysed the cells in RIPA buffer (25 mM Tris pH 7.6, 150 mM NaCl, 1 % NP40, 1 % Na-deoxycholate, 0.1 % SDS) and incubated on ice for 15 min. Lysates were cleared of insoluble material by centrifugation at 15,000 rpm. We determined the protein concentration by Bradford assays and loaded 15 μg of total protein per sample. To perform subcellular fraction Western blot analyses, we collected aliquots for each fraction and loaded equivalent amounts for each fraction (see mNET-seq methods section for fractionation protocol). Denatured proteins were separated by denaturing gradient gel electrophoresis (4-20 %, Life technologies) and transferred to a nitrocellulose membrane (GE Healthcare Life Sciences). Western blotting was performed with standard protocols. Antibodies used for detection of proteins in the lysates are listed in the key resources table.

TT-seq

We performed TT-seq as previously,[55,82] described here in brief. We treated 30 million cells per biological replicate sample. Following treatment, we metabolically labeled the cells for 5 min with 500 μM 4-thiouridine (4sU). The cells were then pelleted and lysed in Qiazol (Qiagen). The lysates were spiked-in with three 4sU-labeled and three 4sU-unlabelled synthetic RNAs. Total cellular RNA was then isolated according to standard protocols followed by fragmentation, sonication and biotinylation of the 4sU-containing RNA. Two biotinylation reactions were set up per sample (150 μg fragmented total RNA, 10 mM Tris pH 7.5, 1 mM EDTA pH 8.0, 200 μg/ml HPDP-biotin, 40 % DMSO) and pooled following purification with the μMACS Streptavidin Kit (Miltenyi). The 4sU-labeled RNA, eluted with 100 mM DTT, was purified and concentrated with the miRNeasy Micro kit (Qiagen). 100 μg of the purified 4sU-labeled RNA was used as input for the Stranded Total RNA Prep with Ribo-Zero Plus (Illumina). The libraries were checked on the Fragment Analyzer before pooling and paired-end sequencing with 75 cycles on a NextSeq 550 (Illumina).

mNET-seq

We performed mNET-seq as previously,[55] described here in brief. We treated 50 million cells per biological replicate sample. To isolate the chromatin, we followed the protocol as described by Nojima et al.[56] The chromatin pellets were then washed with MNase buffer and digested with MNase (NEB) for 2 minutes at 37 °C. The reactions were then centrifuged to remove insoluble debris. To prevent co-precipitation of splicing intermediates or other co-transcriptional processing products, we included empigen (Sigma) in the binding and washing buffers.[83] The supernatant was diluted with 1:10 NET-2E buffer (50 mM Tris-HCl (pH 7.4, 150 mM NaCl, 0.05 % (vol/vol) NP-40 and 1 % Empigen BB). We added 75 μl of antibody-conjugated beads (Dynabeads M-280 Sheep Anti-Mouse IgG prebound with 7.5 μg anti-CTD antibody (Diagenode)) and incubated in the cold room for 1.5 h. The beads were washed 6 times with NET-2E buffer and the RNA was phosphorylated at 5' RNA ends with T4 PNK 3' phosphatase minus (NEB). We eluted the RNA with RNA extraction buffer (ZYMO Quick-RNA microPrep kit). *S. cerevisae* mRNA spike-ins were prepared as

Please cite this article in press as: Žumer et al., FACT maintains chromatin architecture and thereby stimulates RNA polymerase II pausing during transcription *in vivo*, Molecular Cell (2024), https://doi.org/10.1016/j.molcel.2024.05.003

previously described.[55] We added 100 pg of fragmented spike-in to the extraction buffer. Next, short immunoprecipitated RNA fragments were size selected (< 200 nt) and purified from the eluates according to the manufacturers protocol (ZYMO Quick-RNA microPrep kit) and eluted in 7.5 μl nuclease-free water. We took 1 μl to check the RNA quality with Fragment Analyzer (Agilent) and proceeded to the NGS library preparation with Truseq small RNA library preparation kit (Illumina). We purified the DNA with the Monarch kit (NEB) and separated the DNA on a 4 % E-Gel (HR, Invitrogen) and performed library size-selection to 150 - 230 nt. NGS libraries were quality checked and quantified with the Fragment Analyzer (NGS kit). The samples were pooled and sequenced paired-end with 43 cycles on the NextSeq 550 (Illumina).

MNase-seq

We performed MNase-seq with 1 million K562 cells per biological replicate. After centrifugation and washing the cells with cold DPBS we resuspended the cells in 120 μl hypotonic buffer (10 mM HEPES pH 7.4, 2 mM $MgCl_2$ and 0.5 % NP40; supplemented with protease inhibitor cocktail (Sigma)) on ice and incubated 5 minutes. Next we added 0.4 μl micrococcal nuclease (2,000,000 gel units/ml, NEB), heated up to 37 °C, added $CaCl_2$ to a final concentration of 2 mM and incubated at 37 °C for 4 minutes before adding one volume of 2x Stop solution containing 20 mM Tris–HCl pH 8, 4 mM $MgCl_2$, 300 mM NaCl, 20 mM EDTA, 3 mM EGTA, 2 % SDS, 0.2 μg/μL RNase A, and 3 ng/μl *D.melanogaster* mononucleosomes (spike-in DNA). The samples were then incubated at 37 °C for 30 minutes, followed by addition of 200 μg proteinase K (Thermo Scientific) and 15 minutes of incubation at 55 °C. The DNA fragments were then purified by phenol:chloroform:IAA extraction and precipitation with isopropanol. The digestion time was optimized beforehand to yield ~80 % mononucleosomes and ~20 % dinucleosomes. The spike-ins were prepared with the same protocol using 5 min digestion of 50 million S2 cells with 0.25 μl of micrococcal nuclease. Spike-in mononuclesomes were purified by separating the fragments on a 4 % E-Gel (HR, Invitrogen) and performed size-selection by excising the smear between 90 – 200 nt. NGS libraries were prepared with the NEBNext Ultra II DNA Library Prep Kit for Illumina (NEB) according to manufacturer's instructions. The NGS libraries were quality checked and quantified with the Fragment Analyzer (NGS kit) and pooled for sequencing paired-end with 43 cycles on the Illumina NextSeq 550.

5'cap-seq

We performed sequencing of 5' ends of capped mRNAs (5'cap-seq) as described previously[55] with modifications. Described here in brief, we treated 25 million cells per samples for 1 or 4 h with dTAG7 or solvent only (DMSO). Next, we spiked the samples with *D. melanogaster* S2 cells (1:10) and performed subcellular fractionation as for mNET-seq. The chromatin pellets were treated with DNase I for 10 min before lysis in Qiazol (Qiagen). For each biological sample, 5 μg of RNA were treated with 5 U of Turbo DNase (Ambion) for 20 min at 37 °C. The RNA samples were then treated with 1 U of Terminator 5'-Phosphate-Dependent Exonuclease (Epicentre) for 60 min at 30 °C and purified by phenol:choroform:IAA extraction. rRNA-depleted RNA was treated with 30 U of quick CIP (NEB) for 30 min at 37 °C and purified by double-phenol extraction and phenol:choroform:IAA extraction. CIP-treated RNA was then incubated with 5 U of Cap-CLIP acid pyrophosphatase (Cellscript) for 60 min at 37 °C. Decapped-RNA samples were then purified by phenol:choroform:IAA extraction and ligated overnight at 16 °C with an RNA adapter (10 μM) containing an 8-mer molecular barcode (UMI), 1 μl of T4 RNA ligase 1 and ATP (1 mM) for ligation to the 5' ends of RNA. The following day, the samples were purified with 2X volume of RNAclean XP beads (Beckman Coulter) according to the manufacturer's instructions followed by RNA fragmentation with NEBNext Magnesium RNA Fragmentation Module (NEB) for 5 min at 80 °C, and immediately transferred on ice. Fragmented samples were purified with 3.5X volume of RNAclean XP beads and then incubated with random hexamers (Invitrogen) and dNTPs for 5 min at 65 °C, followed by incubation on ice. The RNA was reverse transcribed with Superscript II (Invitrogen) (25 °C for 10 min, 42 °C for 50 minutes, inactivation at 70 °C for 15 minutes). cDNA samples were purified with Ampure XP beads (Beckman Coulter). cDNA second-strand was synthesized with 0.5 μL of 5 μM biotinylated primer and Phusion High-Fidelity PCR Master Mix with HF Buffer (NEB) (1 min at 98 °C, 2 min at 50 °C and 15 min at 72 °C), followed by purification using Ampure XP beads.

The library preparation was performed as previously described.[55,84,85] The obtained libraries were analyzed with the Fragment Analyzer (NGS kit). Followed by pooling and size-selection with Ampure XP beads to obtain fragments between 200 and 700 bp. The NGS libraries were sequenced on the Illumina NextSeq 550 to generate 75-bp single-end reads.

ChIP-seq

We performed sequencing of chromatin immunoprecipitation sequencing (ChIP-seq) as described previously[57] with minor changes. 180 million cells from 2 biological replicates were treated with DMSO or dTAG7 ligand for 1 or 4 h, before they were crosslinked with 1% formaldehyde for 8 min. 125 mM Glycine was added to quench the reaction and samples were incubated for 5 min at room temperature. Cells were washed twice with ice-cold DPBS. A pellet containing 30 million cells was lysed with 5 mL of lysis buffer (5 mM Pipes pH 8.0, 85 mM KCl, 0.5% NP-40, 1x protease inhibitor (Sigma-Aldrich), 1x phosphatase inhibitor (Sigma-Aldrich)) for 10 min on ice. Samples were centrifuged at 1,700 g for 5 min at 4 °C and washed once with ice-cold DPBS. Nuclei pellet was resuspended with 1 mL of sonication buffer (10 mM Tris-HCl pH 7.5, 1mM EDTA, 0.4% SDS, 1x protease inhibitor, 1x phosphatase inhibitor) and incubated on ice for 10 min. Samples were transferred to AFA milliTubes and chromatin shearing was done using S220 Focused-Ultrasonicator (Covaris) with following settings: duty cycle 5%, peak incident power 140W, cycle per burst 200, processing time 900 sec, bath temperature 6 °C, degassing mode continuous, water level (Run) 8. Sonicated chromatin was centrifuged at 10,000 g for 15 min at 4 °C. Each chromatin sample was checked for size distribution using 1% agarose gel electrophoresis.

50 μL of Th1L (NELF-C/D) antibody (Cell Signaling Technology), 20 μL of Rpb1 NTD antibody (Cell Signaling Technology) were coupled to Dynabeads Protein G (Invitrogen) together with 2 μL of histone H2Av antibody (Active Motif). Samples containing 100 μg of chromatin were mixed with 600 ng of sheared chromatin from *D. melanogaster* S2 cells, and 1:8 diluted with immunoprecipitation (IP) buffer (56.25 mM Tris-HCl pH 7.5, 157.5 mM NaCl, 1 mM EDTA, 1.125% Triton X-100, 0.1125% Na-deoxycholate, 1x protease inhibitor, 1x phosphatase inhibitor). Before dilution, 1% of samples was taken for input control samples and stored at 4 °C. The diluted IP samples were incubated with bead-coupled antibodies overnight at 4 °C on a rotating wheel. The following day the beads were washed 5 times with LiCl wash buffer (100 mM Tris-HCl pH 7.5, 500 mM LiCl, 1% NP-40, 1% Na-deoxycholate) and once with TE buffer (10 mM Tris-Hcl pH 8.0, 1 mM EDTA). Elution of immunoprecipitated chromatin was performed twice with 100 μL of elution buffer (100 mM NaHCO3, 1% SDS) at 70 °C for 10 min. Elution buffer was added to input samples to adjust the volume to 200 μL. IP and input samples were reverse crosslinked overnight at 65 °C. Samples were treated with RNase A for 1.5 h at 37 °C and with proteinase K for 2 h at 45 °C. DNA extraction was performed using 1 volume of phenol:chloroform:isoamyl alcohol 25:24:1 and Phase Lock Gel tubes. DNA was precipitated overnight at -20 °C by addition of 200 mM NaCl, 1 μL of Glycogen and 2.5 volumes of 100% ethanol. DNA pellets were washed with 70% ethanol and resuspended in 30 μL of H2O. DNA library preparation was performed according to NEBNext Ultra II DNA Library Prep Kit for Illumina (NEB). Quality of the library and size distribution was checked on Fragment Analyzer. Samples were pooled and paired-end sequenced with 43 cycles.

Tiled-MCC

Tiled-MCC libraries were generated as previously described.[49] Briefly, 20 × 10^6 cells per biological replicate were crosslinked with 2% formaldehyde and permeabilized with 0.0025% digitonin (Sigma-Aldrich, D141). The fixed cells were subsequently digested with Micrococcal nuclease (MNase, NEB, M0247) in triplicate titration reactions ranging from 50-70 Kunitz U of MNase in a low Ca^{2+} reaction buffer (10 mM Tris-HCl pH 7.5, 10 mM $CaCl_2$) for 1 h at 37 °C. In preparation for DNA ligation, the digestion reactions were first quenched with 5 mM ethylene glycol-bis(2-aminoethylether)-N,N,N′,N′-tetraacetic acid (EGTA) (Sigma-Aldrich, E3889), a 10% aliquot was then further processed for digestion efficiency; samples with 70-80% of the fragments corresponding to mono-nucleosomes (∼180 bp) were selected for the subsequent steps. DNA end-repair and ligation reactions were performed consecutively in the same tube with 200 U mL^{-1} T4 polynucleotide Kinase (NEB, M0201), 100 U mL^{-1} DNA polymerase I large (Klenow) fragment (NEB, M0210), and 300 U mL^{-1} T4 DNA ligase (Thermo Scientific, EL0013) in a DNA ligase buffer (Thermo Scientific, B69) supplemented with 0.4 mM dNTP mix (NEB, N0447) and 2.5 mM EGTA, in a thermomixer using a pre-set program at 37 °C for 2 h followed by 20 °C overnight. The ligated product was de-crosslinked and purified using DNeasy blood and tissue kit (Qiagen, 69504). To eliminate the un-ligated material, one-sided size-selection was performed using AMPure XP beads (Beckman Coulter, A63881). The samples were further processed for sonication to reach an average fragment size of 200 bp, followed by indexing using NEBNext ® Ultra ™ II DNA Library Prep Kit for Illumina (NEB, E7645). For the tiled enrichment, a custom panel of biotinylated oligos targeting the regions of interest was designed using a python-based oligo tool[86] (https://oligo.readthedocs.io/en/latest/). The biotinylated oligos were resuspended in the hybridization mix (Twist Hybridization and Wash Kit, Twist Bioscience, 101025) and pooled together with the pre-mixed dried DNA of the indexed samples resuspended in a human-specific blocker solution and universal blockers. The hybridization reaction was incubated for 16 h at 70 °C. Following streptavidin bead pulldown and several washes, the samples were subjected for 11 amplification cycles of post-hybridization PCR. The quality of the PCR-amplified and purified libraries was checked on a Fragment Analyzer (Agilent). The samples were sequenced using a 150-bp paired-end kit on the NextSeq550 Illumina platform. MCC[87] (https://github.com/jojdavies/Micro-Capture-C) and HiC-Pro[88] (https://github.com/nservant/HiC-Pro) pipelines were used for data analysis as previously described.[49]

QUANTIFICATION AND STATISTICAL ANALYSIS

Sequencing data preprocessing

All sequencing data was demultiplexed with Illumina tools and then quality checked with FastQC (http://www.bioinformatics.babraham.ac.uk/projects/fastqc/). TT-seq reads were trimmed with Cutadapt[74] with options: -f fastq -q 30 -m 25 -O 13 -a AGATCGGAAGAGCACACGTCTGAACTCCAGTCAC -A AGATCGGAAGAGCGTCGTGTAGGGAAAGAGTGTAGATCTCGGTGGTCGCCGTATCATT, followed by mapping to the human genome version GRCh38 merged with the synthetic RNA spike-in sequences[53] with the STAR mapper[75] with options: –runThreadN 24–readFilesCommand zcat –outFilterType BySJout –outFilterMultimapNmax 1 –alignSJoverhangMin 8 –alignSJDBoverhangMin 1 –outFilterMismatchNmax 999 –outFilterMismatchNoverLmax 0.02 –alignIntronMin 20 –alignIntronMax 1000000 –alignMatesGapMax 1000000 –outSAMtype BAM SortedByCoordinate. Duplicates were marked with Picard tools (http://broadinstitute.github.io/picard). We then kept only uniquely mapped and properly paired reads for the downstream analyses. The counts from spike-ins were then used to generate normalization factors for the human gene counts and coverage profiles.

The mNET-seq reads were trimmed with Cutadapt[74] with options: -f fastq -q 30 -m 20 -O 13 -a TGGAATTCTCGGGTGCCAAGGAACTCCAGTCAC -A GATCGTCGGACTGTAGAACTCTGAAC followed by mapping to the human genome version GRCh38 merged with the yeast genome version SacCer3 with the STAR mapper[75] with options: –runThreadN 24–readFilesCommand zcat –outFilterType BySJout –alignEndsType Extend5pOfReads12 –outFilterMatchNminOverLread 0.80 –outFilterMultimapNmax 1 –alignSJoverhangMin 8 –alignSJDBoverhangMin 1 –outFilterMismatchNmax 999 –outFilterMismatchNoverLmax 0.02 –alignIntronMin 20 –alignIntronMax 1000000 –alignMatesGapMax 1000000 –outSAMtype BAM SortedByCoordinate. Duplicates were marked with Picard tools. We kept only uniquely mapped and properly paired reads to identify the last incorporated base (3' end of the RNA), which is

the first mapped base in read 2, and used only this position in downstream analyses. The counts for yeast genes were used to generate normalization factors with DESeq2[89] to normalize the coverage profiles.

MNase-seq were trimmed with Cutadapt[74] with options: -f fastq -q 30 -m 25 -O 13 -a AGATCGGAAGAGCACACGTCTGAACTCCAGTCAC -A AGATCGGAAGAGCGTCGTGTAGGGAAAGAGTGTAGATCTCGGTGGTCGCCGTATCATT, followed by mapping to the human genome version GRCh38 merged with the *D. melanogaster* genome version Dm6 with the Bowtie2 mapper[78] with options: –no-unal–no-mixed –no-discordant –very-sensitive –seed 123 –threads 24. Duplicates were marked with Picard tools. We then kept only uniquely mapped and properly paired reads for the downstream analyses. The counts mapping to the spike-in genome were below 1 % and were therefore not used for normalization. We corrected for differences in library sequencing depth with normalization factors based on numbers or reads that mapped to non-transcribed regions in the human genome. These normalization factors were then used for normalization of the human gene counts and coverage profiles. We took the midpoints of the fragments to get the positions of the putative nucleosome dyads. The dyad positions were then smoothed using normal kernel density smoothing with a bandwidth of 75 bp. These smoothed dyad coverages were then used to generate metagene profiles. Nucleosome positions were also determined with the DANPOS tool.[44] We utilized the comparative analysis tool to quantify the occupancy and fuzziness changes for the individual treatment times.

The 5'cap-seq reads were first trimmed of the UMI (first 8 nt of the reads) with UMI-tools[77] and then trimmed with Cutadapt[74] with options: -f fastq -q 30 -m 25 -O 13 -a AGATCGGAAGAGCACACGTCTGAACTCCAGTCAC followed by mapping to the human genome version GRCh38 merged with the *D. melanogaster* genome version Dm6 with the STAR mapper[75] with options: –runThreadN 24 –readFilesCommand zcat –outFilterType BySJout –outFilterMultimapNmax 1 –alignEndsType Extend5pOfRead1 –alignSJoverhangMin 8 –alignSJDBoverhangMin 1 –outFilterMismatchNmax 999 –outFilterMismatchNoverLmax 0.05 –alignIntronMin 20 –alignIntronMax 1000000 –alignMatesGapMax 1000000 –outSAMtype BAM SortedByCoordinate. We next deduplicated the mapped data with UMI-tools to remove any PCR duplicates based on the UMI sequences. We then identified the first transcribed base (5' end of the RNA) and used only this position in downstream analyses. The spike-in reads (processed as above) that mapped to the *D. melanogaster* genome were too low to be used for robust normalization, so we used reads mapping to human genes to obtain normalization factors to correct for sequencing depth and therefore refrain from performing expression change analyses for this dataset.

ChIP-seq data was checked for quality using FastQC, and reads were aligned to human hg38 genome assembly merged with *D. melanogaster* genome using Bowtie2[78] with the following parameters: -p 24 –no-discordant –no-mixed –very-sensitive. Duplicates were removed using Picard tools (http://broadinstitute.github.io/picard).

We determined the gene set for downstream analyses by first filtering know-gene RefSeq reference annotation (RefSeq sequence database[90]) to remove overlapping genes and then selected genes that had median RPK >10 for all control samples. This yielded 8970 expressed genes, which we used for downstream analyses. Preprocessed data was analyzed in RStudio utilizing R version 4.2.3 and packages from the Bioconductor repository[72,73] and Tidyverse.[76] All plots were generated with ggplot2.[91]

Differential gene expression analyses

First we collected the counts per expressed gene for each of the TT-seq samples with the findOverlaps package (Bioconductor[72,73]) using options: ignore.strand = FALSE, singleEnd = FALSE, mode = "IntersectionNotEmpty". The sizeFactor parameter was set to the spike-in normalization factor and differential gene analyses were performed with the DESeq2 package[89] with the *padj* cutoff set to 0.05, which corresponds to 5 % false discovery rate. MA plots were generated with ggplot2.[91]

Estimation of elongation velocity

To estimate the change in elongation velocity we determined the ratio between RNA synthesis and RNA Pol II occupancy (TT-seq/mNET-seq) as described previously.[55] In brief, to determine the TT-seq/mNET-seq ratio we determined the midpoints of each mapped TT-seq read-pair (fragment). These were then transformed to coverage and normalized with the corresponding normalization factor. We tiled the genome into 50bp-bins and determined the sum of coverage TT-seq fragment-midpoints and mNET-seq coverage in each bin to then generate the ratio per bin. For visualization of changes in elongation velocity in heatmaps we determined the ratio of treated to control per bin.

Metagene profiles and heatmaps

Coverages were generated from uniquely mapped and properly paired TT-seq reads or last incorporated base of mNET-seq for each strand and normalized with their corresponding normalization factor. For MNase-seq the coverage was generated from the smoothed dyad signal. Replicates of treatment conditions were combined by summing the normalized coverages per nt. Coverage windows were then collected for the loci of interest. To generate plots aligned at two points, the intervening region was scaled by binning the coverage into 600 bins and 200 bins for the upstream and downstream flanking regions (±2 kb). We determined the mean per bp/bin and it's 0.05 to 0.95 confidence interval (CI) by bootstrap method with 10,000 repetitions. For unscaled metagene profiles we determined the mean and CI per nucleotide. Metagene profiles were plotted with ggplot2.[91]

To generate heatmaps we determined changes in signal per bin (50 nt). Bins without coverage in either condition/experiment were treated as missing data and assigned the value "NA". Heatmaps with mean of the signal per bin were generated for the indicated range. Regions with no signal (NA) are show in light gray. The color scale range is indicated, values above and below the range are squished into the range. Heatmaps showing ratios have log transformed color scales. Heatmaps profiles were plotted with ggplot2.[91]

Determination of transcription start sites (TSS), pause sites and +1 nucleosome positions

We determined the TSSs of expressed genes with a constitutive start site. We identified the site of maximum 5'cap-seq signal within 25 bp upstream and 250 bp downstream of the reference annotation start (hg38 NCBI RefsSeq known-genes) for the sense strand of the 1 h DMSO treated control (SSRP1-dTAG, combined replicates). We obtained 4838 TSSs and used these as the TSS in downstream analyses.

We determined the pause sites for RNA Pol II in expressed genes with a constitutive TSS by calling maximum peak of mNET-seq signal in the window 250 nt downstream of the TSS or the first exon excluding the last bp (exons < 250 nt) for the sense strand of the 1 h DMSO treated control (SSRP1-dTAG, combined replicates). We then retained only pause sites that were above 3 times the median of non-zero values in the same window to remove low signal sites. With these criteria we obtained 5832 pause sites with a median distance of 45 bp downstream of the TSS.

To determine the positions of the +1 and -1 nucleosome dyads, we determined nucleosome positions as described in Žumer et al.,[55] but from the experimentally determined TSSs. We then subset the annotations to genes that had all four positions determined (n = 4681) and used these for all downstream analyses.

Quantification of subnucleosomal fragments

We quantified subnucleosomal fragments by splitting mapped MNase-seq fragments into subsets by fragment length. The 80 – 120 bp fragments correspond to partially unwrapped nucleosomes and 140 – 180 bp fragments correspond to mono-nucleosomes. We next determined the number of fragments that map to regions of interest. To control for any biases in fragment size distribution between the samples we determined size factors based on the total number of the respective fragments per sample, which corrects also for sequencing depth, and used these size factors to normalize the fragment counts. We report the normalized fragments counts per genomic region in fragments per kilobase.

Estimation of intragenic drop-off probability p

For a gene of length L, we assumed p is the independent uniform gene-specific probability of drop-off from any base between TSS and the TES. RNA synthesis signal across the gene body would be constant when there is no drop-off (p=0) of RNA Pol II throughout the gene. An increase in drop-off would result in lower RNA synthesis (TT-seq) per base towards 3' ends of genes compared to 5' ends of genes (first 3 kbp). The loss of the signal can be represented as a negative binomial probability of drop-off which theoretically scales exponentially with the length of the gene L.

$$drop\text{-}off\ ratio\ =\ (1\ -\ p)^{\left(\frac{L}{2}-1\right)}$$

To obtain the drop-off ratio, we determined the ratio of mean per base RNA synthesis (TT-seq) in the gene body (cov_f, [TSS + 3 kbp, TES]) and the 5' end of genes (cov_i, [first 3 kbp]). We determined the mean RNA synthesis by calculating the mean TT-seq fragment midpoints per basepair. We use L/2, which corresponds to the midpoint of a gene, in our formula above as a scaling factor instead of L to account for the use of average RNA synthesis per basepair.

$$drop\text{-}off\ ratio\ =\ \frac{cov_f}{cov_i}$$

Estimation of p using this method has been done for n=3190 genes, which passed the criterion that $cov_i > cov_f$ and L > 3.5 kbp.

Quantification of in vitro RNA elongation assay products and barrier indexes

RNA products (intermediates °, °°, and full-length product) were quantified using Fiji's integrated density values.[92] Raw intensity values and box sizes are reported in the Table S2. Normalization was performed to control for variations during gel loading and other external and non-transcription related factors. To normalize RNA product signals, we first subtracted the background signal from signal intensity from the full-length RNA extension products, followed by normalization against the sum of the transcribed signal of the respective lane (excluding the excess of RNA primer).

The entry and dyad barrier indices were calculated as visualized in Figure S5D. The RNA extension intermediate product signal (at the barrier) and the cumulative signal of all RNA products that were extended beyond the barrier (signal above the intermediate RNA product signal) of the respective lane were normalized by subtracting the background. Next, the normalized RNA extension intermediate product signal was divided by the sum of the RNA extension intermediate product signal and the normalized cumulative signal of all RNA products that were extended beyond the barrier (Figure S5D). Graphs were rendered in Prism 9 (GraphPad Software).

Replicates and statistics

All treatments were performed in two biological replicates to generate sample NGS libraries. Biochemical assays were performed in triplicate. Numbers of genes/features analyzed and statistical test are indicated in the corresponding figure legends. The error bars, statistical tests and representations are described in the respective figure legends.